united nations
educational, scientific
and cultural
organization

international atomic
energy agency

the
abdus salam
international centre for theoretical physics

SMR/1328/17

School on the Physics of Equatorial Atmosphere

(24 September - 5 October 2001)

Propagation effects of Plasma

M. A. Abdu
(Instituto Nacional de Pesquisas Espaciais, São José dos Campos, Brazil)

Propagation effects of Plasma (M.A. Abdu)

(Reflection – Ionospheric sounding, data interpretation; group delay –GPS applications, TEC; Amplitude and phase scintillations as related to structures; ISR fundamentals) (M.A.Abdu)

Introduction

A large part of the ionospheric investigations has been, and continue to be, based on propagation effects on radio waves in plasma. The earliest known of such effects was the reflection of radio waves at a conducting boundary, which made possible the discovery, of the ionosphere, and the determination of the height of the reflecting layers, by Appleton and Barnett (1924) and Briet and Tuve (1925). The pulsed technique of radio wave sounding of the ionosphere first introduced by the latter authors continues to be the most widely used technique in ionospheric research and monitoring to the present day.

A radio wave propagating in the ionospheric plasma is subject to the following effects.

-Total reflection,
-Partial reflection,
-Refraction- phase advance, group delay,
-Change of polarization,
-Absorption,
-Scattering- coherent scattering, incoherent scattering.

The predominant effects suffered by a radio wave vary with its frequency in relation to the plasma frequency and gyro frequency of the magnetized plasma in which it propagates. By appropriate selection of the probing radio wave frequency a specific effect or a combination of effects, mentioned above, can be made use of to investigate the ionosphere.

1- Ionospheric sounding by pulsed radio waves- Ionosonde technique

An ionosonde is basically a sweep frequency HF radar and it measures the electron density distribution as a function of height as a most basic parameter. The electron density at a given height in the ionosphere is determined from the plasma frequency at which a radio wave is reflected. The height of reflection is determined from the time measured for a pulsed radio wave to travel vertically to the ionosphere and back to the point of its reception (the receiver and the transmitter being located at the same point for vertical sounding of the ionosphere). An ionosonde transmits into the ionosphere sequential pulses of radio waves in such a way that a given pulse reflected by the ionosphere is received back before the next pulse is transmitted. The electron density of the ionosphere increases with height, reaches a maximum and then decreases upward. Therefore the frequency of an ionosonde is swept from a lower frequency, usually 1 MHz, which is less than the day time plasma frequency at the lower limit of the ionosphere, approximately 95 km in the E region, (which is the usual sensitivity limit of an ionosonde), up to 20 MHz that exceeds the top plasma frequencies of the ionosphere in the F region. An ionosonde located on the ground measures the electron density

distribution at the bottomside of the ionosphere, whereas a satellite based sounder can provide the density distribution of the topside of the ionosphere.

A radio wave propagating into the ionosphere is reflected back at a height where its phase refractive index becomes zero. This condition is expressed, using the simplified expression for the refractive index as follows:

$$\mu^2 = 1 - X = 1 - \omega_p^2/\omega^2$$

Here $\omega = 2\pi f$, $\omega_p^2 = (2\pi f_p)^2 = N_e e^2/\varepsilon_0 m$ (proportional to the electron density N_e).
(This expression neglects the effect of earth's magnetic field and electronic collision with neutral particles).
When ω_p exceeds ω, μ becomes imaginary and the wave does not propagate. The wave gets reflected at $\omega_p = \omega$., Since

$$f_p^2 = 80.5\ N_e \quad (f_p \text{ is in Hz and } N_e \text{ is in } m^{-3}).$$

the reflected wave thus yields the electron density.

The height of the reflection point is determined from the time it takes for the radio wave pulse to travel the two-way path which is the delay (τ) between the transmitted and received pulses recorded by the instrument.

Assuming that the pulse travels with the velocity of light the height of reflection is given by:

$$h' = c\tau/2 \qquad (1),$$

In fact the pulse travels with the group velocity , v_g which is related to the speed of light by the group refractive index, μ' as: $v_g = c/\mu'$.
In (1) c should be replaced by v_g that varies with height. Thus

$$\tau = 2\int_0^{h_r} \frac{dh}{v_g} = 2\int_0^{h_r} \frac{\mu}{c} dh \qquad (2)$$

Eq. (1) becomes:

$$h' = \int_0^{h_r} \mu' dh$$

In fact the virtual height (or the group height) h' and the real height h_r the real height at which a given frequency is reflected are connected by an equation that depends on the electron density distribution below the reflection point, since n' is a function of f and N_e. Thus:

$$h' = \int_0^{h_r} \mu'(f, N_e) dh$$

As shown by Ratcliff (1959), for negligible magnetic field the group refractive index is given by: $\mu' = 1/\mu$.

Since $\mu' > 1$, h' is higher than the real reflection height h_r as illustrated in the following figure.

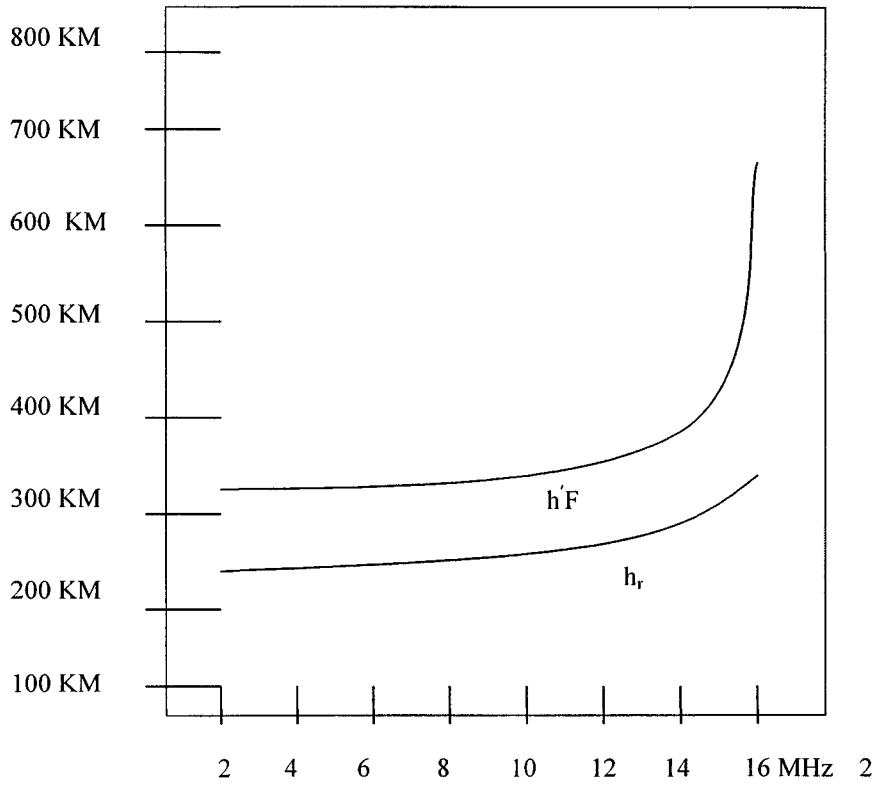

Fig. 1

To get the height distribution of the plasma frequency (that is, electron density) in a specific ionospheric layer such as that shown in **Fig.1** above the ionosonde sweeps the frequency from a low value (usually 1 MHz) upward. Increasing frequencies are reflected at higher levels of increasing density until the frequency becomes equal to that of the plasma frequency at the peak of the layer. Radio waves of higher frequencies penetrate the layer. The highest frequency reflected by a layer is called the critical frequency of the layer Usually the ionosonde frequency is swept from 1 MHz to 20 MHz, which covers the largest critical frequencies, observed of the F layer of the ionosphere. At the point of the layer penetration the radio waves remain longer time in the layer, because the group velocity tends to be zero, resulting in a large increase in h' (f) shown by the infinite slope (also known as a cusp) of the trace as illustrated in the above figure. An example of a highly idealized ionogram for a multiple layer ionosphere (with the corresponding plasma frequency profile in the inset) is shown in **Figure 2.**

An example of real ionogram is shown in **Fig. 3.** These ionograms show that the h' (f) curve is split into traces, called ordinary and extraordinary. To understand this phenomenon we need to consider the original Appleton – Hartree equation that include

the effect of earth's magnetic field (and collision of electrons with the neutrals) as given below:

$$\mu^2 = 1 - \frac{X(1-X)}{(1-X) - \frac{1}{2}Y_T^2 \pm \left[\frac{1}{4}Y_T^4 + (1-X)^2 Y_L^2\right]^{1/2}} \qquad (3)$$

Where $X = \omega_p^2/\omega^2$; $Y = \omega_H/\omega$; $\omega_H = 2\pi f_H = (e/m)B_0$

$Y_L = Y\cos\theta$, $Y_T = Y\sin\theta$

The Eq.3 shows that the effect of the geomagnetic field is to make the ionosphere a doubly refracting medium. Two modes propagate that are characteristic waves known as 'ordinary, and 'extra ordinary' waves corresponding to the '+' and '-' signs respectively. We have seen that a wave vertically incident on the ionosphere is reflected where $\mu^2 = 0$.

For ordinary wave which is equivalent to the case of zero magnetic field, this occurs, as discussed before at X = 1.

For extraordinary wave the reflection occurs at a level where

$$X = 1 - Y \text{ if } Y < 1 \ (\omega_H < \omega)$$
$$\text{and where } X = 1 + Y \text{ if } Y > 1 \ (\omega_H > \omega)$$

If the wave normal is in the direction of the magnetic field ($\theta = 0$) then $Y_L = Y$ and $Y_T = 0$

.

Even when $\theta \neq 0$ a good approximation for n may be obtained by taking $Y_T = 0$. Such a condition generally holds for high frequency waves as long as X is not 1 and θ is not near 90°. (The actual condition for its validity is:

$$\frac{1}{4}Y_T^4 << (1-X)^2 Y_L^2$$

Quasi longitudinal approximation holds for high-frequency waves in the ionosphere provided X is not near 1 and θ is not near 90° . For this case the refractive index is given by:

$$\mu^2 = 1 - X/(1 \pm Y_L)$$

The two modes are nearly circularly polarized in opposite senses, and a plane-polarized wave traversing the ionosphere can be regarded as the sum of "ordinary" and "extraordinary" components. Because the two waves travel with different velocities the plane of polarization continuously rotates as the wave propagate through the ionosphere. This effect is known as Faraday rotation.

At the peak of the layer where N_e is maximum we can get a relationship between the critical frequencies for the ordinary and extra ordinary waves by applying the conditions X = 1 and X = 1- Y,

$f_p{}^2/f^2 = 1$ and $f_p{}^2/f_x{}^2 = 1 - f_H/f_x$; where $f_H = \omega_H/2\pi$ by substitution we get $f_0 = f_H/2$ valid when the critical frequency is much higher than f_H.

On the basis of the above consideration the idealized ionogram of **Fig.2** and the observed ionogram of **Fig.3** can be easily explained. The ordinary and extra ordinary traces are separated in frequency by approximately $f_H/2$ as are the critical frequencies of the different layers.

Examples of ionograms, some from conventional systems with recording in films and some obtained from modern digital technology are shown in the following figures: **Figures 4- 8.** Ionospheric sounding is done also from satellite born sounders. An example of topside ionogram is shown in **Fig.8a**

The ionospheric parameters that are usually scaled from an ionogram and are used for communication purposes, data analysis and ionospheric investigations are given in the following table:

Table-1

Layer Critical Frequencies	**Layer heights**	**Spread F type**
$\mathbf{f_{o,x}F_2}$ – the ordinary or extra ordinary critical frequency of the F_2 layer **M(3000)F_2**	$\mathbf{h_mF_2}$ – the height of the maximum electron density of the F_2 layer ; h'F- minimum virtual height of the F layer	Range spread (**Q**) Frequency spread (**F**)
$\mathbf{f_oF_1}$ –the critical frequency of the F_1 layer	**h'F**- the virtual height of the F_1 layer	
$\mathbf{f_oE}$- the critical frequency of the E layer	**h' E**- the virtual height of the E layer	
$\mathbf{f_oE_{1,2}}$ – the critical frequencies of the E_1 and E_2 layers	**h' $E_{1,2}$** – the virtual heights of the E_1 and E_2 layers	
$\mathbf{f_{o,x}E_s}$ – the ordinary or extra ordinary critical friquencies of the sporadic E layer ; $\mathbf{f_bE_s}$- the blanketing frequency of the sporadic e layer	**h'E_s** – the virtual height of sporadic E layer $\mathbf{E_s}$ layer types- **l, f, c, h, s, q**	

Modern digital ionosondes and their capabilities

Concepts of modern ionosondes: The modern ionosondes operate like a HF Doppler radar system working at a large number of frequencies in sequence. It measures the angle of arrival, polarization and spectrum as a function of range. The ionosonde makes all measurements as a function of sounding frequency to probe the ionosphere the E region to the peak of the F layer. Large array measurements are made possible with a digital system with computerized controls and digital signal processing. The digital ionosonde steps through a selected frequency band in precise frequency increments, and samples

(digitizes) the receiver output in precise time intervals corresponding to virtual height increments or radar range bins. If the sounder operates with F frequencies and H height ranges, the ionosonde data output array consists of F•H data pixels. The value of F is usually of the order of 200 and H will have 128, 256v or 512 values depending upon the height range and height resolution. Each pixel contains all observables of an electromagnetic signal: amplitude, phase, Doppler spectrum polarization, and incidence angle. Fixed frequency observations are made for F = 1, or F = 2, 3, etc. if 2 or 3 frequencies are transmitted in a multiplexed mode. The details of the array dimensions and how the observables are measured and the data processed, interpreted, and stored differ for the various instruments.

The most widely used equipment of this type is the Digisonde (Reinisch, 1995, The digisonde network and databasing, World Data Center A for Solar-Terrestrial Physics, Report UAG-104, Ionosonde Network and Stations, pp. 8-15, 1995). (For other types of digital ionosonde see, J. McDougal et al., 1995, Report UAG-104, The Canadian digital ionosonde:design and results, See also, R. D. Hunsucker, 1991, Radio techniques for probing the terrestrial ionosphere, Physics and Chemistry in Space, 22, Springer Verlag, Berlin).

Capabilities of digital ionosonde:

Real time true height, automatic scaling of key ionospheric parameters, ionospheric drifts in horizontal and veritical directions, echo location, Multi beam ionograms, Precision group height, Interference avoidance and digital gain control. Some examples of these capabilities are presented in Figs. 9a,b, c, e, f, g.

2- Group delay, Phase advance and GPS applications:

Many space application activities utilize transe-ionospherically propagating radio waves emitted by orbiting or geostationary satellites. An example of a most widely used application is the use of GPS (Global Positioning System) satellites for navigation, that is, range and position determination. The information extracted in such application, however, are subject to modification suffered by the radio waves in passing through the ionosphere. This is because the ionosphere is a dispersive medium for radio waves, as it produces frequency dependent refraction on the radio wave passing through it. As a result a modulation envelope (a pulse code) suffers group delay, and the phase of a carrier wave advances, with respect to their free space values. Therefore a precise knowledge of the ionospheric total electron content is necessary to correct for the errors in measurements. On the other hand if the propagation errors could be independently determined by the use of an adequate technique the error information so obtained can provide a means to determine and monitor the total electron content of the ionosphere.

The satellite based radio beacon method is based on measurement by a receiver on ground, or onboard another receiver, the difference of the modulation time delay and/or carrier phases of two coherent frequencies f_1 , f_2 . The principle of the technique is as follows:

The phase advance ϕ of an electromagnetic wave with frequency f is described by:

$$\phi = f\,t - (f/c)\int \mu\, ds \qquad (4)$$

where $\mu = 1 - K/f^2 N_e$

$K = 40.3\ m^3 s^{-2}$

that is, $\phi = (fK/cf^2)\int N_e\, ds \qquad (5)$

$$\int N_e\, ds = TEC \text{ (total electron content)}$$

The differential phase between two frequencies is given by:

$$\Delta\phi = (K/c)\,(1/f_1 - 1/f_2)\,TEC \text{ and}$$

the phase path difference is given by:

$$\Delta P_\phi = K(1/f_1^2 - 1/f_2^2)TEC \qquad (6)$$

When comparing the modulation phase, or code signals, instead of carrier phases, the group refractive index need to be used.

$$\mu_g = 1/\mu = 1 + K/f^2 N_e\ ;$$

The group path at the frequency f is given by:

$$P_g = \int \mu_g\, ds = \int (1 + K/f^2 N_e)\, ds\ ;$$

The group delay $P_{gd} = ct - P_g = -K/f^2 \int N_e\, ds$

The GPS satellites transmit two frequencies in the L-band at $f_1 = 1575.42$ MHz (L_1) and $f_2 = 1227.60$ MHz (L_2). They will be modulated by some code.

The differential group delay between L_1 and L_2 is therefore given by:

$$P_{(L1-L2)} = K(1/f_2^2 - 1/f_1^2)\int N_e\, ds \qquad (7)$$

The integral of the electron density along the ray paths contribute to the total electron content as illustrated in **Fig. 10**.

The time delay suffered by these codes is a measure of the distance from a satellite and the effect from propagating medium (ionosphere + stratosphere) such that $\rho_R^S = ct_R^S$. By measuring the t_R^S by a receiver from from satellites the position of the receiver can be determined as illustrated in **Fig.11**.

The error in t_R^S due to the ionosphere can be determined using the psudo –range and carrier phase measurements as follows:

$$P = \rho + c(dt - dT) + d_I + d_T + d_M + \varepsilon_p \qquad (8)$$

$$\phi = \rho + c(dt - dT) - d_I + d_T + \lambda N + \varepsilon_c \qquad (9)$$

Where

P = psudo range
ρ = geometric range between satellite and reciever
dt = offset of the satellite clock
dT offset of the receiver clock
d_I = ionospheric range error
d_T = tropospheric range error
d_M = effect of multipath on pseudo range
λ = signal wave length
N = carrier phase ambiguity (cycles)
ε_p, ε_c = residual errors in pseudo range and carrier phase respectively.

(d_M is negligibly small , in mm range, for phase measurement, but in meters for pseudo range).

The difference in pseudo range (group path) between the L-band frequencies L_1 and L_2 from (8) and the difference in carrier phase path from (9) are given by:

$$P_{g2} - P_{g1} = K\,(1/f_2^2 - 1/f_1^2)\,TEC + \Delta\varepsilon_p' \qquad (10)$$

$$P_{\phi 1} - P_{\phi 2} = K\,(1/f_2^2 - 1/f_1^2)\,TEC + \lambda_1 N_1 - \lambda_2 N_2 + \Delta\varepsilon_c' \qquad (11)$$

The $\Delta\varepsilon'$ terms include unmodelled residuals and random errors. In the case of carrier phase measurements there are also unresolved phase cycle ambiguities that need to be resolved by special algorithm.

These equations can be used to:
1- remove first order ionospheric propagation error from the position measurement on L_1 , and
2- derive the electron content along the considered ray path.

Considering the previous equations the ionospheric range error at L_1 GPS frequency is directly proportional to TEC and amounts to $d_I = 1.62 \times 10^{-7} TEC$ which results in typical ionospheric range errors of several meters.

The GPS dual frequency technique is widely used for regional and global ionospheric TE C monitoring and investigation of ionospheric phenomenology. Assuming a single layer model of the ionosphere having an effective height h_{sp} , the measured slant TEC, TEC_s can be converted into vertical columnar content TEC_v by the following relation:

$$TEC_v = \sqrt{1 - \left(\frac{h_{sp}\cos\varepsilon}{h_{sp} + r_E}\right)^2}\; TEC_s$$

Where r_E is the earth's radius, ε is the elevation angle, and height of the ionospheric shell is usually assumed to be around 400 km. Some examples of the TEC mapping results are shown in **Fig.12.**

3- Diffraction of radio waves: scintillation development

As a radio wave travels through an irregular medium it will accumulate small changes of amplitude and phase which will be different at different points of the wave front as illustrated in **Fig. 13.** The figure shows a simple case of a plane wave front incident on a phase-changing thin screen, which introduces small (<1 radian) phase perturbation along the wave front. The emerging wave front is irregular as shown by EE′. The field at the observing plane OO′ will also be irregular as both the amplitude and phase are affected and the received field strength at point P is the sum of the contribution from points such as 'a' and 'b'. The observation at the ground can be used to deduce information about the wave front leaving the ionosphere and to use it to deduce information about the irregularities. There is no one-to-one relationship between the irregularities in the ionosphere and in the wave field at the ground, but there is relationship of statistical nature.

According to diffraction theory most of the signal strength is due to contribution from the first Fresnel zone. By definition the first Fresnel zone extends to the point where the distance to the observer exceeds the minimum distance by $\lambda/2$ (the resulting phase difference being 180°). This is given by $(\lambda D)^{1/2}$ known as the radius of the Fresnel zone. When the observing point is close to the phase screen such that the first Fresnel radius is smaller the typical irregularity sizes the amplitude fluctuation will be small and slow. When the distance of the observing point is long enough so that the Fresnel radius contain several typical irregularity sizes the amplitude fluctuation will be stronger and more rapid. An example of amplitude scintillation is shown in **Figure 14.** The figure shows also some statistics of the fades.
The intensity of scintillation is quantified by means of an index; the most widely used being the S4 index defined as:

$$S_4 = \left(\overline{P^2} - \overline{P}^2\right)^{1/2} / \overline{P}$$

P is the received power. This simply is the standard deviation of received power normalized by the mean value. Another method, less precise is to measure the range in decibels below the third peak from the highest to the third dip from the lowest on the record. S_4 varies as $\lambda^{1.5}$ for small values ($S_4 < 0.6$) For large values of S_4 (> 0.6, or peak-to-peak scintillation exceeding 10 db) the wave length dependence vanishes. Index of phase scintillation varies as λ except under most extreme conditions.

Structure sizes from fading:

The spectrum of fading is of interest to deduce the structure sizes responsible for the scintillation. The irregularities in the ionosphere generally show a power law spectrum of the form k^{-p}, k being the spatial wave number ($2\pi/\lambda_e$), λ_e being the spatial wavelength of the irregularities. The pattern of amplitude and phase fluctuation over the ground produce by the movement of the phase screen is related to the spectrum of these irregularities themselves. The largest power in the amplitude spectrum arises from those irregularities that have scale sizes of the order of a radius of the first Fresnel zone $(\lambda D)^{1/2}$. This is shown by Fig.15. The corresponding frequency is called Fresnel frequency ν_F given by: $\nu_F = u/(2\lambda D)^{1/2}$ (the denominator being defined as Fresnel wave length). D being the distance to the receiver from the diffraction screen.

Thus if we assume a value for the height of the irregularities (D) we can infer the velocity of the irregularity structure. In **Fig.15** $\nu_F = 0.16$ Hz. If we assume D=350 km, for λ = 12m, the horizontal velocity is given by: $u = 109\ ms^{-1}$. On the other hand if we have an independent determination of the velocity, such as that can be obtained from a spaced receiver observation of fading, we can calculate the effective height of the structure. A spaced receiver technique involves measurements at two ground stations separated in East-West direction for structures aligned along magnetic field line in North-South direction. A cross correlation between the amplitudes fluctuation at the two antennas (separated by a distance, d, which is usually a few hundred meters) can yield the time delay between the maxima or minima of the diffraction pattern observed at the two antenna. If τ_d is the time delay the velocity component in the direction of the antenna base line is given by $v_d = d/\tau_d$ .In general 3 or more spaced receivers are used in an experiment to get the horizontal velocity vector.

4- Incoherent scatter fundamentals

In coherent scatter, also known as "Thomson scatter" technique is a powerful tool for studying ionosphere. It is the only ground based technique capable of observing all the regions (bottom and top sides) of the ionosphere. The incoherent scattering of radio waves arises from fluctuation in electron density having a scale of the Debye length in the plasma defined as:

$$\lambda_D = (\varepsilon_0 k T_e/N_e^2)^{1/2} = 69\ (T_e/N_e)^{1/2} \quad m.$$

This is the distance within which an electron in the sphere of influence of an ion acts independently of other ions.

The basic theory is developed from consideration of the reradiation of incident electromagnetic energy by free electrons. As originally shown by J.J. Thomson, in 1906, the energy scattered by a single electron per unit solid angle per unit incident flux is given by: $W = (r_e \mathrm{Sin}\Psi)^2$, where re is the classical electron radius given by : $r_e = e^2/\varepsilon_0 m_e c^2 = 2.82\times10^{-15}$ m. , Ψ is the angle between the electric vector of incident electromagnetic wave and the direction from electron to the observer. e and m are respectively the charge and mass of the electron. ε_0 is the permitivity of free space and c is the velocity of light. The radar cross section is given by: $\sigma_e = 4\pi(r_e \mathrm{Sin}\Psi)^2$

That is, $\sigma_e = 4\pi r_e^2 = 1.0 \times 10^{-28}\ m^2$ for radar back-scatter.

Since electrons are in 'random' thermal motion the power radiated by the electrons will add at the receiver so that the radar cross-section per unit volume is simply: $\sigma_R = N_e \sigma_e$
An example of the power received from a scattering region: A volume of 3 km diameter and 20 km long with 10^{12} electrons/m^3 has $1.4x10^{11}$ x 10^{12} electrons. The total scatter cross-section is 1.4×10^{-5} m^2 which is equivalent to a sphere of approximately 2 mm. In the lower ionosphere for a cylinder of 1 km diameter and 1 km long the cross-section becomes ~ 0.78×10^{-9} m^2 equivalent to a sphere of radius of 0.016 mm.

The detection of scattered signals from such regions/objects require high power transmitter system, large antenna, most sensitive receiver and very sophisticated data processing system that all add up to a major facility. The back scattered returned power is given by (see, Hunsucker, Radio Techniques for probing the terrestrial ionosphere, Springer- Verlag, 1991):

$$P_s = (\mu_0 e^4/16\pi^2 m_e^2 c)(E_0^2 N_e/r^2) = 2.1 \times 10^{-32} E_0^2 N_e/r^2$$

Where, $N = N_e V$ is the total number of electrons in a volume V contributing to the received signal;

r is the distance of the scattering volume from the transmitter;
E_0 is the electric field produced by the transmitter in the scattering volume;
μ_0 , m_e, e and c are the standard constants.

To have an idea on the intensity of the scattered signal, the following example can be considered:

Transmitter power = 10^6 W;
Antenna gain = 46 dB (0.6°beam width);
r = 200 km; $N_e = 3 \times 10^{11} m^{-3}$.

The scattered power at the receiver is $Ps = 2 \times 10^{-19}$ W m^{-2} .With the antenna collecting aperture of $700m^2$

The received power = 1.4×10^{-16}W

Which is comparable to the noise power of a receiver with 100K noise temperature and 100 kHz bandwidth. The usual practice to take the difference of the receiver noise from the received power and integrate the difference for significantly long time, of the order of 1 min. An example of the first electron density profile of the ionosphere is shown in **Fig. 16 a, b and c.**

Gordon (Proc. IRE 46, 1824, 1958) predicted that the thermal motion of the electron would produce Doppler spectrum with Guassian distribution having half width of about 0.71 Δf_e , where Δf_e the Doppler shift is given by : $\Delta f_e = 2v/\lambda$, where $v = (2kT_e/m_e)^{1/2}$

Where v is the mean thermal speed; λ is the radar wavelength; k is the Boltzmann's constant; T_e , m_e, are temperature and mass of electrons.
Expressing the wave length in meters $\Delta f_e = 11\ T_e^{1/2}/\lambda$ kHz;
Using typical values as T_e = 1600 K

λ = 75 cm (for f = 400 MHz) we get

$$\Delta f_e = \sim 600 \text{ kHz}$$

However, the observed spectrum was 200 times narrower than this. The explanation for such narrow spectrum was that although the scattering comes from the electrons the motion of the electron is controlled by ions. The use of ion mass in the equation for Δf_e reduces its value by $(m_i / m_e)^{1/2}$. If for example, the ion is O^+ this ratio is 170. The extend to which the ions control the electron motion depends on the radio wave length in relation to the Debye length as was theoretically shown by Dougherty and Farley, (1960, A theory of incoherent scatter of radio waves by a plasma, Proc. R. Soc. Lond.,A 259, 79, 1960).

If $\lambda < \lambda_D$ the motion seen are controlled by electron temperature and mass. If $\lambda > \lambda_D$ which is generally the case with all the existing ISR, the scattering is due mainly to irregularities of electron density fluctuation controlled by ions. In fact radar observes an assembly of irregularities each the size of a Debye length moving at the ionic thermal speed.

$$\text{Thus } \Delta f_i = (8kT_i/m_I)^{1/2}/\lambda = 65T_i^{1/2}/\lambda \text{ Hz}$$

For O^+ ions $T_I = 1600$ K and $\lambda = 75$ cm, $\Delta f_i = 3.5$ kHz

For $\lambda < \lambda_D$ the radar can see electron lines, not controlled by ions. In the general case both lines are present. Buenman (JGR, 67, 2050, 1962) showed that the effective radar cross section (σ_{eff}) can be written as $\sigma_{eff} = \sigma_e/[(1+\alpha^2)(1+T_e/T_I + \alpha^2)]$, and the ratio of the power in the electron and ion lines is:

Electron line power / ion line power $= \alpha^2(1+T_e/T_I + \alpha^2)$. A typical spectrum is shown in **Fig.17.**

A more detailed treatment of the spectrum involves consideration of fluctuation within the medium as a spectrum of waves, ion-acoustic and electron acoustic waves. These waves occur over a wide range of wavelengths and propagate in all direction. Back-scatter will occur from these ion-acoustic waves whose wavelength equals half the incident radio wave. Two such waves exist one moving away, and one towards, the transmitter. The resulting Doppler shifts are $\pm F(\Lambda)$ where,

$$F(\Lambda) = (1/\Lambda)[(kT_i/m_i)(1+T_e/T_i)]^{1/2}$$

The expression in square bracket is velocity which is close to the speed of the ions. This leads to a spectrum with two lines with separation proportional to $(T_i/m_i)^{1/2}$. When $T_e = T_i$ $\Lambda = \lambda/2$ this formula is the same as that obtained for simple case of ion m_i . The theoretical form of the ion spectra for different values of T_e/T_i are shown in **Fig.18**

Parameters that can be measured by incoherent scatter technique:

Electron density: - From total power returned from the scattering region. Usually absolute density is not obtained. Some comparison with ionosonde is made to get the density profile.

- From frequency offset of the plasma line and also from Faraday effects.

T_e/T_i ratio: - From the ratio of the peak to dip in the spectrum.

T_i/m_i ratio: - From the separation of the peaks (in the ion acoustic region). If m_i is known T_i can be found and hence T_e

Plasma velocity: - Bulk plasma drift in the line of sight produces a Doppler shift of the whole spectrum. By observing in three directions the velocity vector can be determined.

Relative motion of ions and electron: - This makes the spectrum asymmetrical, one peak being higher than the other.

The parameters that can be deduced are: - Conductivity
Neutral wind
Neutral air temperature
Gravity waves
Electron precipitation.

Fig.19 shows global distribution of the existing ISR systems.

Figure Captions:

Fig. 1- An example of an idealized electron density profile of a single layer ionosphere and the expected h' (f) curve from such a profile.

Fig.2- Highly idealized ionogram corresponding to the plasma frequency profile in the inset. The critical frequencies f_oE, f_oF_1, and f_oF_2, correspond to the plasma frequencies of the local maxima in the plasma frequency profile. The extra ordinary trace would not normally be seen at frequencies below about 4 MHz because of absorption.

Fig.3- Digital ionogram with auto scaling (black trace). O traces are plotted in red, X echoes in green. Real time electron density profile is plotted in black giving plasma frequency versus height. The most important autoscaled parameters are listed on the left (from Reinisch, 1996).

Fig.4- Summer and winter noon ionograms for Huancayo Peru, which is almost on the dip equator (dip = 1.2° N. Both ionograms show range spread equatorial Es layer known as E_{sq} .

Fig. 5- Three hours of ionograms form the equatorial station Huancayo, Peru showing the variety of E_s traces. Equatorial E_s (E_{sq}) occurs at 1400, 1415, 1515, 1530, 1600,1615 and 1630. Slant E_s occurs at 1400, 1415, 1530, 1600, 1630 and 1645. After UAG Report 10.

Fig. 6- Ionograms sequences from Fortaleza showing the development of equatorial spread F in the post sunset hours (from Abdu et al., J. Geophys. Res., 86, 6836-6842, 1981).

Fig. 7- Midnight ionogram for Thule, Greenland, dip=85.8°. The extremely spread traces are typical of high latitude spread F. After AGU Report 10.

Fig. 8- Digisonde ionogram for magnetically quiet conditions at Goose Bay, Labrador (dip =76.9°). The ionogram traces have been automatically identified and scaled by ARTIST, and a plasma frequency profile reduced.

Fig.8a- An example of topside ionogram.

Fig.9- (a) An example of automatically scaled ionogram, (b) An example of a multi-beam ionogram, (c) Sky map produced by a digisonde, (d) Sky map for different local times, (e)Azimuth vs UT of the echo locations made by a digisonde, (f) Drift velocity measured by a digisonde compared with plasma velocity measured by nearby, (g) isoelectron density lines produced by the Digissonde –ARTIST software showing the possible gravity wave activity.

Fig.10- Ray path geometry for trans-ionospheric satellite signals. The mapping function $M(\varepsilon) = TEC_s/TEC_v$ is derived using a single layer approximation for the ionosphere. The intersection of the ray path ionospheric shell at the height h_{sp} defines the location (sub-ionospheric point) of the measurement.

Fig.11- Principle of positioning with GPS(Jakovsky, 1996 Modern Ionospheric Science, Ed. Kohl, Ruster, Schlegel, European Geophys. Union) .

Fig.12 Some examples of TEC mapping using global GPS data.

Fig.13- Diffraction of a plane wave incident on a phase-changing screen (Hargreaves, Solar-Terrestrial Environment, Cambridge Uni. Press, 1992).

Fig.14-a- An example of amplitude scintillation, plotted as intensity against time. b- Cumulative probability distribution, c- distribution of fade duration (Handbook of Geophys. And Space Environment, ed. A. S. Jursa, AFGL, 1985).

Fig.15-Amplitude power spectrum for the data recorded on September 6, 1977 over Natal, Brazil (Yeh, et al., JGR, 86, 7527, 1981)

Fig.16-a-Output of integrator used in Bowles' ISR experiment; b- One of the first electron density profiles of the ionosphere obtained using the ISR technique. (Bowles, 1958, Phys. Rev. Letts. 1, 454, 1958), (c) Electron density profie up to high altitudes as measured by Jicamarca radar.

Fig.17- Ion spectrum and plasma (electron) line for conditions $N = 10^{12}$ m^{-3} , $T_e = T_i$ = 1000, λ = 1 m, M = 16. (W. J. G. Byenon and P. J. S Williams, Rep. Progr.Phys. 41, 909, 1978)

Fig.18- Dependence of ion Velocity distribution spectrum on T_e / T_i (W. J. G. Byenon and P. J. S Williams, Rep. Progr.Phys. 41, 909, 1978).

Fig.19- Global distribution of incoherent scatter radar system (ISR) that are operational now. (The MU radar in Shigaraki, Japan, and Gadanki, India, are MST radars capable of being operated as ISR).

Some useful references:

J. K. Hargreaves, The solar-terrestrial environment, Cambridge University |Press, 1992

J. A.Ratcliffe, The magneto-Ionic Theory and its Application to the Ionosphere, Cambridge University Press, Cambridge, UK, 1959.

W. J. G., Beynon and P.J.S. Williams, Incoherent scatter of radio waves from the ionosphere, Report on Progress in Physics, 41, 909, 1978.

K. Davis, Ionospheric Radio , Perigrinus, London (1990).

H. Rishbeth and O. K. Garriott, Introduction to Ionospheric Physics, Academic Press New York and London (1969).

J. V. Evans, Theory and Practice of Ionosphere Study by Thomson Scatter Radar, Proceedings of the IEEE, vol. 57, No.4, , page 496, April 1969.

B.W .Reinisch, Modern Ionosondes, Modern Ionospheric Science, A Collection of Articles Published on the Occasion of the Anniversary:"50 Years of Ionospheric Research in Lindau", Ed. H. Kohl, R. Ruster, K. Schlegel, Max-Panck-Institut fur Aeronomie, European Geophysical Society, Katlenburg-Lindau, FRG 1996.

N. Jabowski, TEC Monitoring by Using Satellite Positioning System, Modern Ionospheric Science, A Collection of Articles Published on the Occasion of the

Anniversary:"50 Years of Ionospheric Research in Lindau", Ed. H. Kohl, R. Ruster, K. Schlegel, Max-Panck-Institut fur Aeronomie, European Geophysical Society, Katlenburg-Lindau, FRG 1996.

R. W. Schunk and A. F. Nagy, Ionospheres, Physics, Plasma Physics, and Chemistry, Cambridge University Press, 2000.

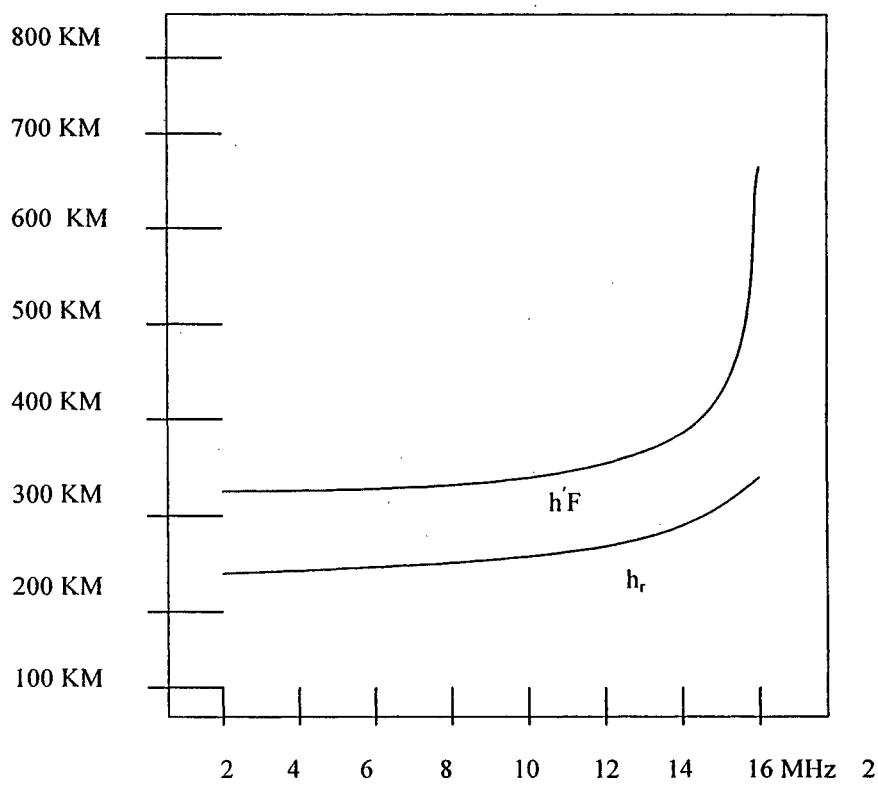
800 KM
700 KM
600 KM
500 KM
400 KM
300 KM
200 KM
100 KM
h'F
h_r
2
4
6
8
10
12
14
16 MHz
2

Fig. 1

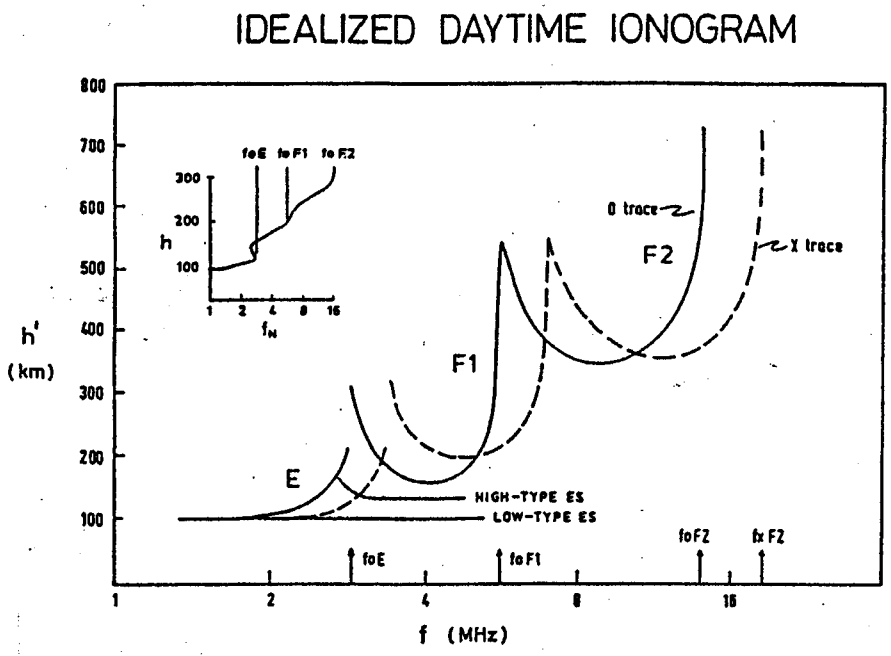

Figure 5.4 Highly idealized ionogram corresponding to the plasma frequency profile in the inset. The critical frequencies f_oE, f_oF_1, and f_oF_2 correspond to the plasma frequencies of the local maxima in the plasma frequency profile. Note that the extraordinary trace would not normally be seen at frequencies below about 4 MHz because of absorption. 1-2

Fig. 02

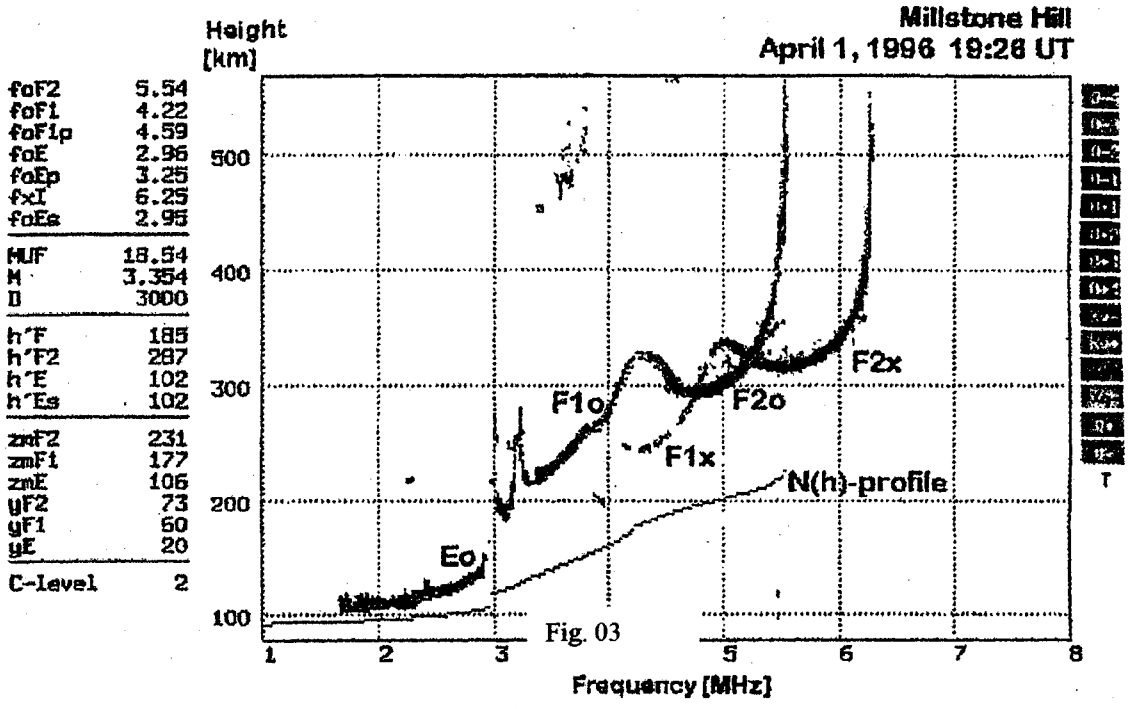

Fig. 03

Digital ionogram with autoscaling (black trace), O echoes are plotted in red, X echoes in green. Millstone Hill, Massachusetts, 1 April 1996, 1426 LT. Real time electron density profile is plotted in black giving plasma frequency versus height. The most important autoscaled parameters are listed on the left,

Fig. 03

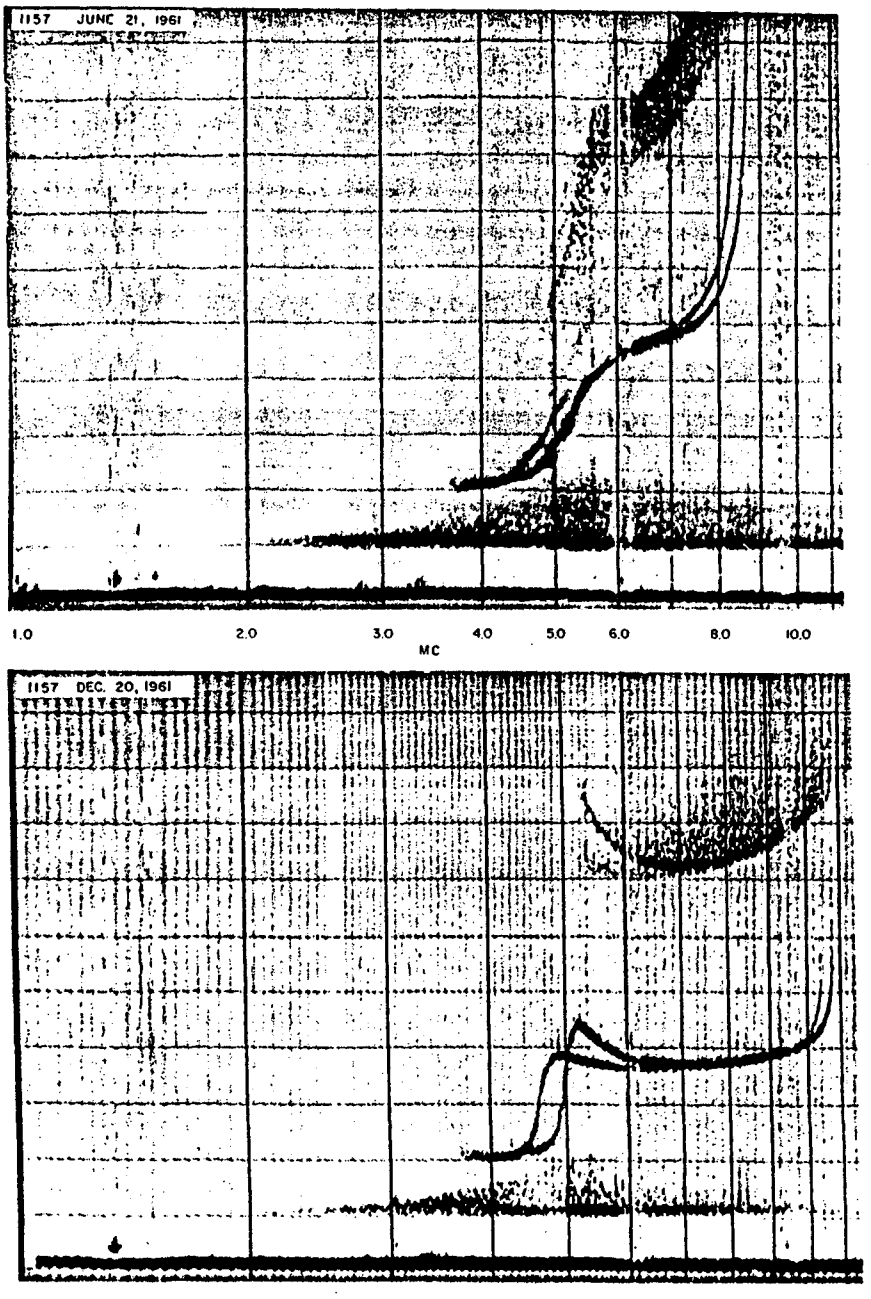

.7 Summer and winter noon ionograms for Huancayo, Peru, which is almost on the dip equator (dip = 1.2° N) ge-spread equatorial E_s at a height of 100 km. *After UAG Report 10.*

1-24

Fig. 04

Es TYPES q and s TYPES
HUANCAYO July 27, 1961

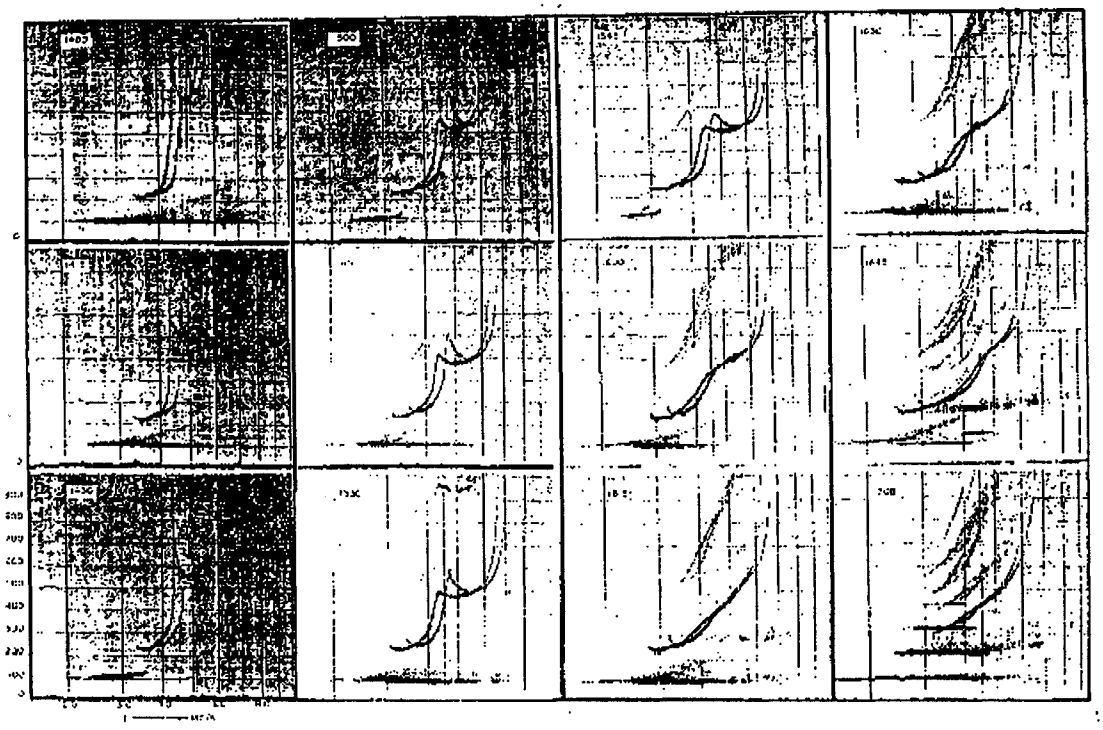

Three hours of ionograms from the equatorial station Huancayo, Peru, showing the incredible variety of E_s traces observed at that station. Equatorial E (E$_{eq}$) occurs at 1400, 1415, 1515, 1530, 1600, 1615, and 1630. Slant E occurs at 1400, 1415, 1530, [illegible]

Fig.05

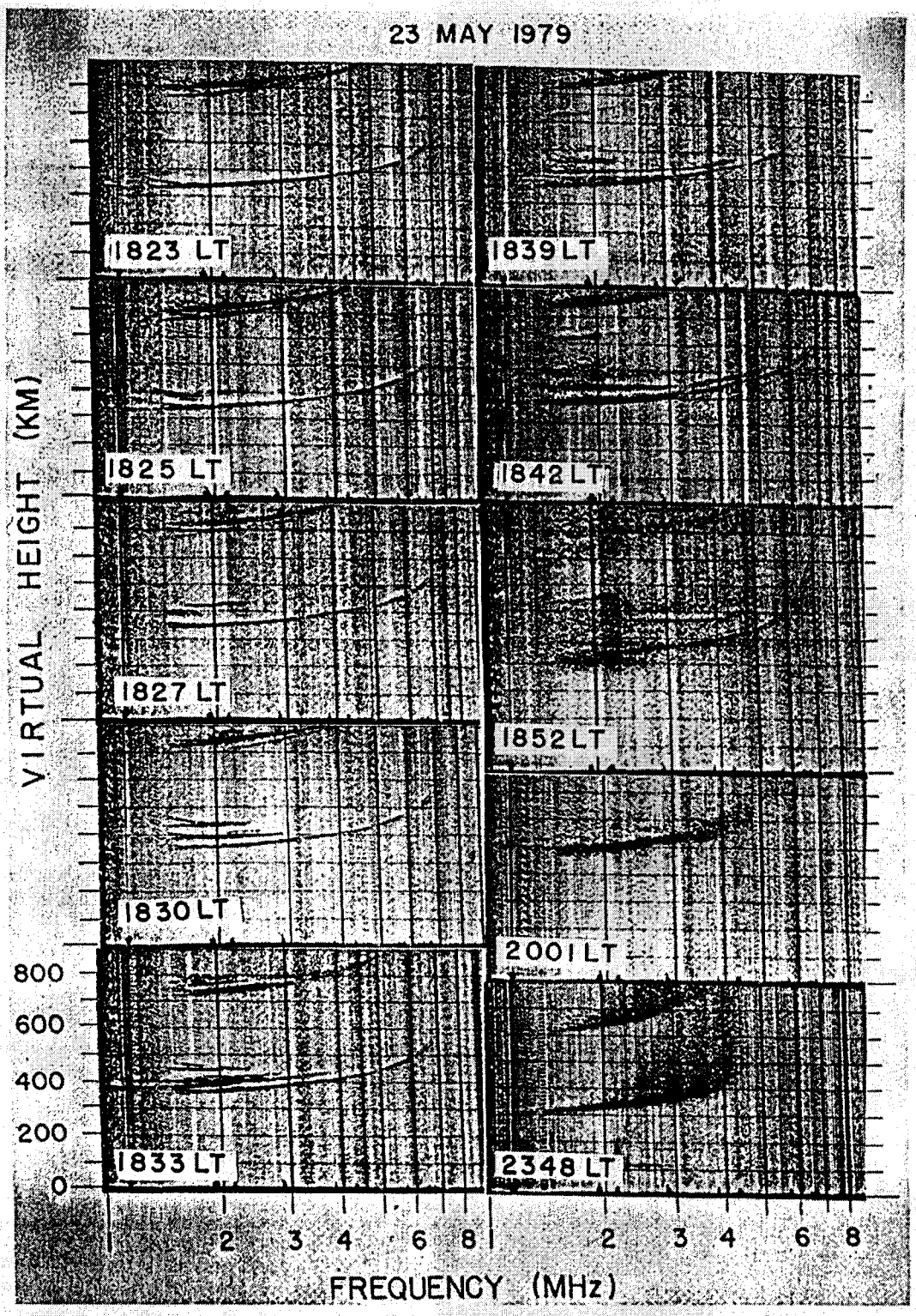

A sequence of ionograms showing the time evolution of the 'satellite' trace from its first appearance adjacent to the low-frequency end of the first-order F trac (at 1823 LT) to the fully developed range type spread (at 1852 LT).

Fig. 06

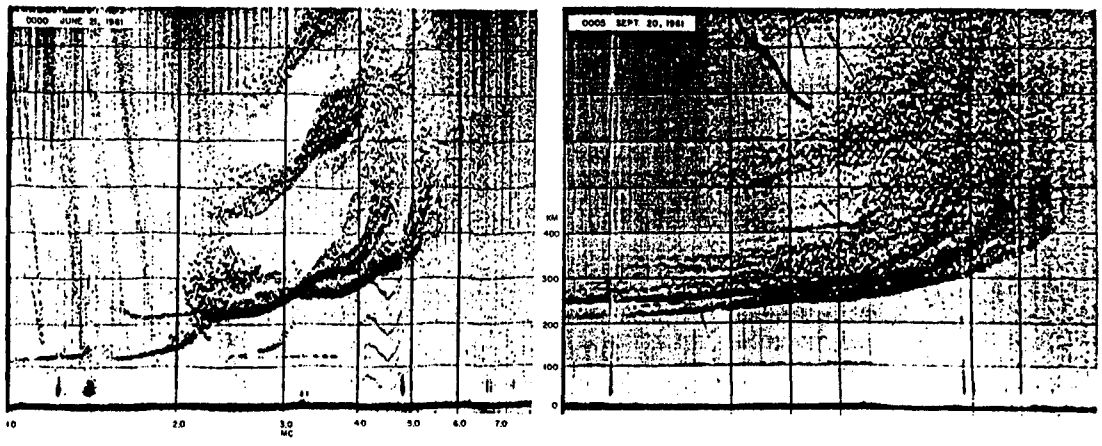

Midnight ionograms for Thule, Greenland, dip = 85.8°. The extremely spread traces are typical of high latitude spread F. *After UAG Report 10.*

Fig. 07

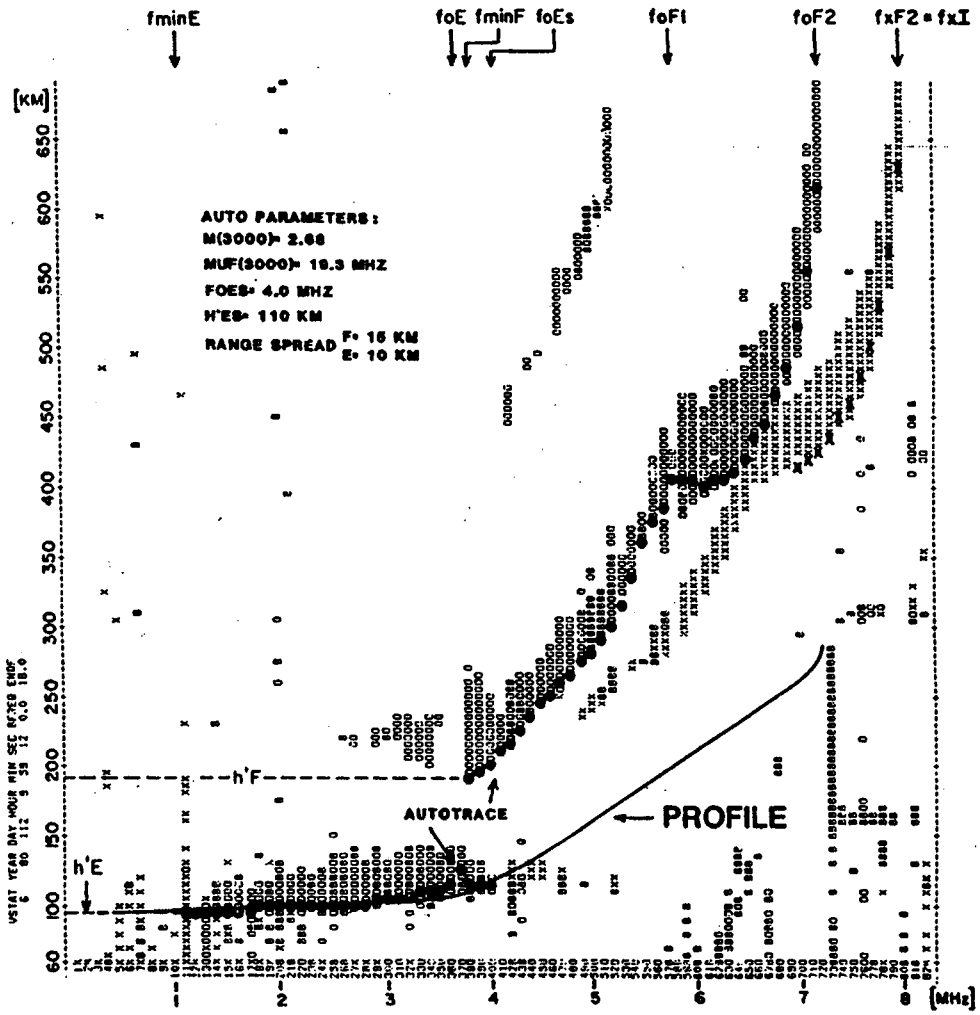

Figure 5.11 Digisonde ionogram for magnetically quiet conditions at Goose Bay, Labrador (dip = 76.9°). The ionogram traces have been automatically identified and scaled by ARTIST, and a plasma frequency profile deduced. *Courtesy University of Lowell Center for Atmospheric Research.*

Fig. 08

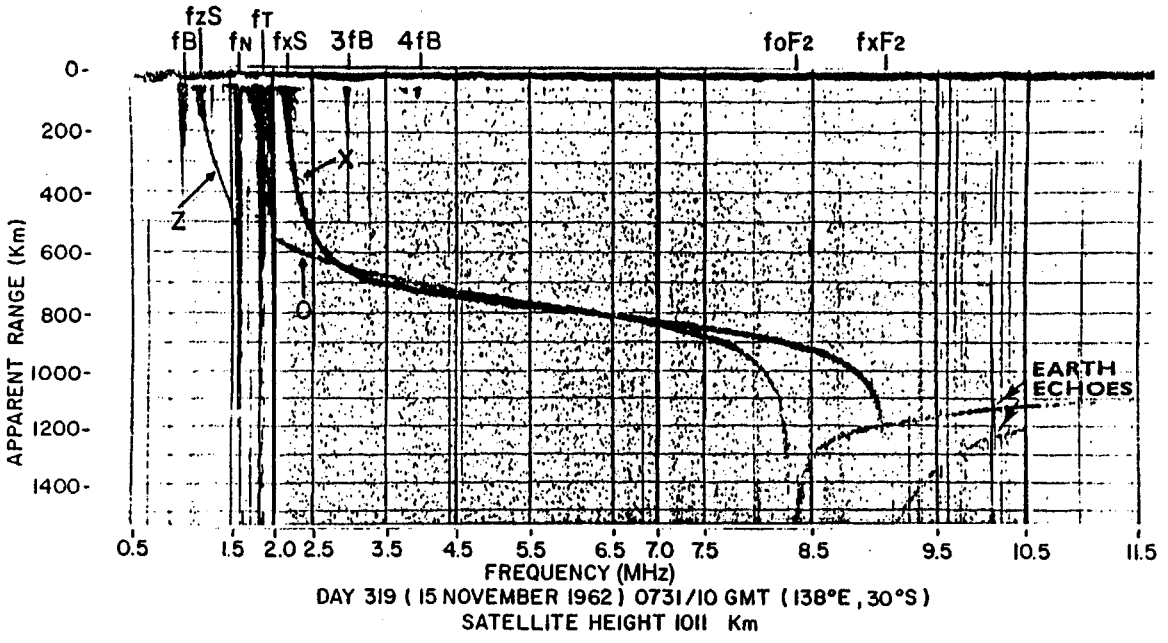

Figure 5.2 A topside ionogram obtained with the Alouette I satellite. A topside ionogram can provide the plasma and gyro frequencies at the satellite, as well as the apparent range (time delay) as a function of frequency. Observed values of f_0F_2, including the only direct observations over the large expanses of ocean, have been used to generate worldwide maps of that parameter.

Fig. 08a

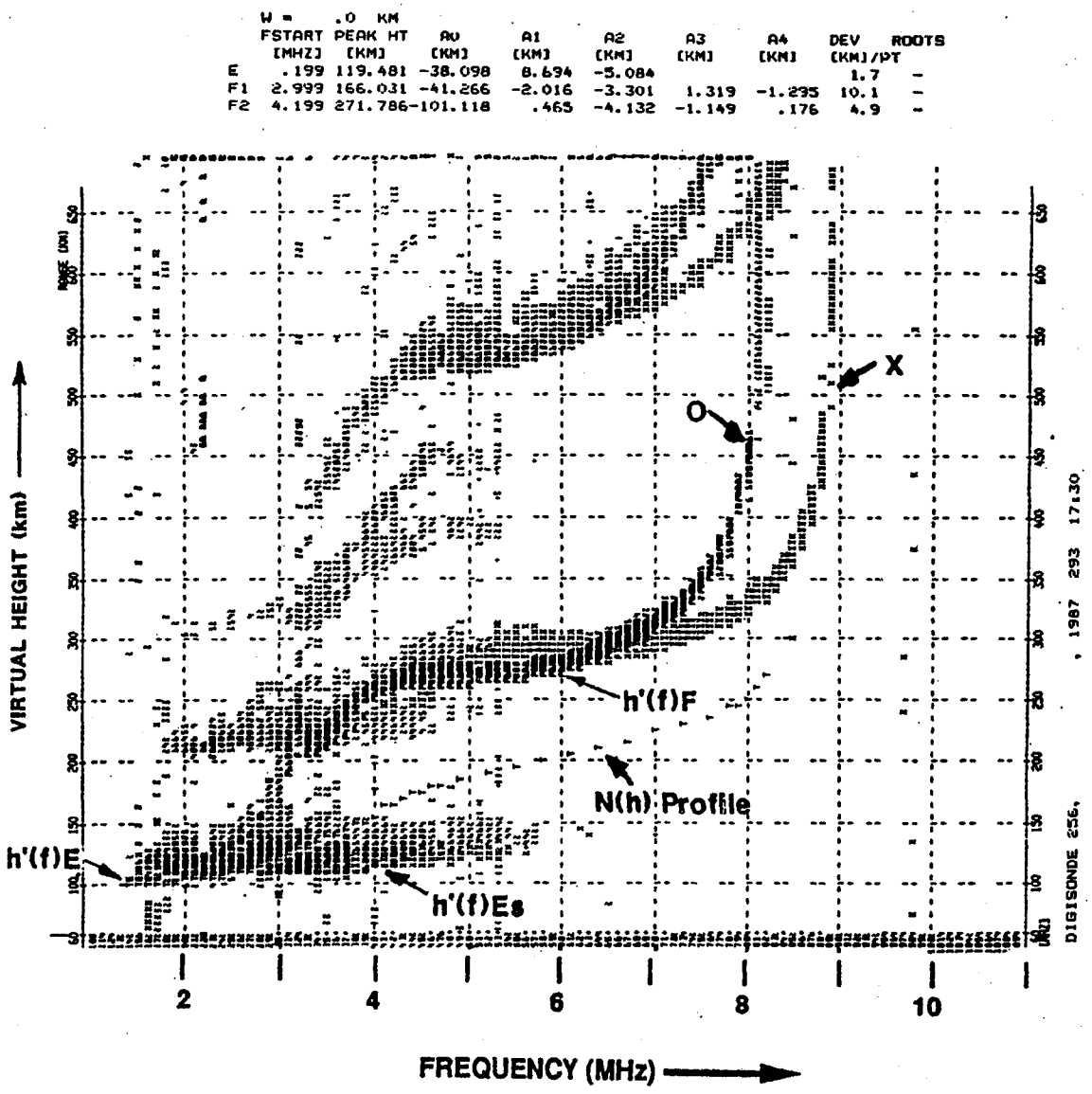

Automatically scaled Digisonde ionogram

Fig. 09a

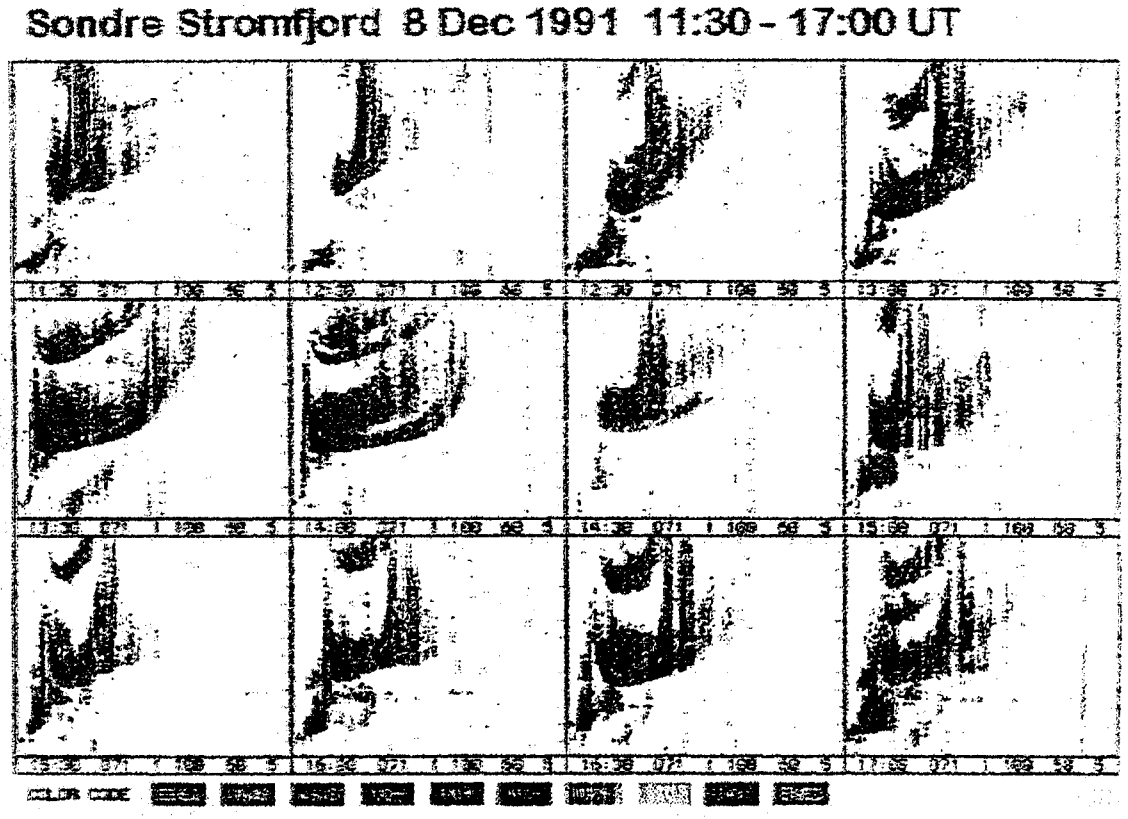

Half hour sequence of multi-beam ionograms at Sondre Stromfjord, Greenland, starting at 1130 UT in the upper left corner and proceeding to the right. The O echoes are plotted in red (overhead), yellow (south), dark blue (north), violet (west-north-west), blue (east-south-east). All X echoes are plotted in green.

Fig. 09b

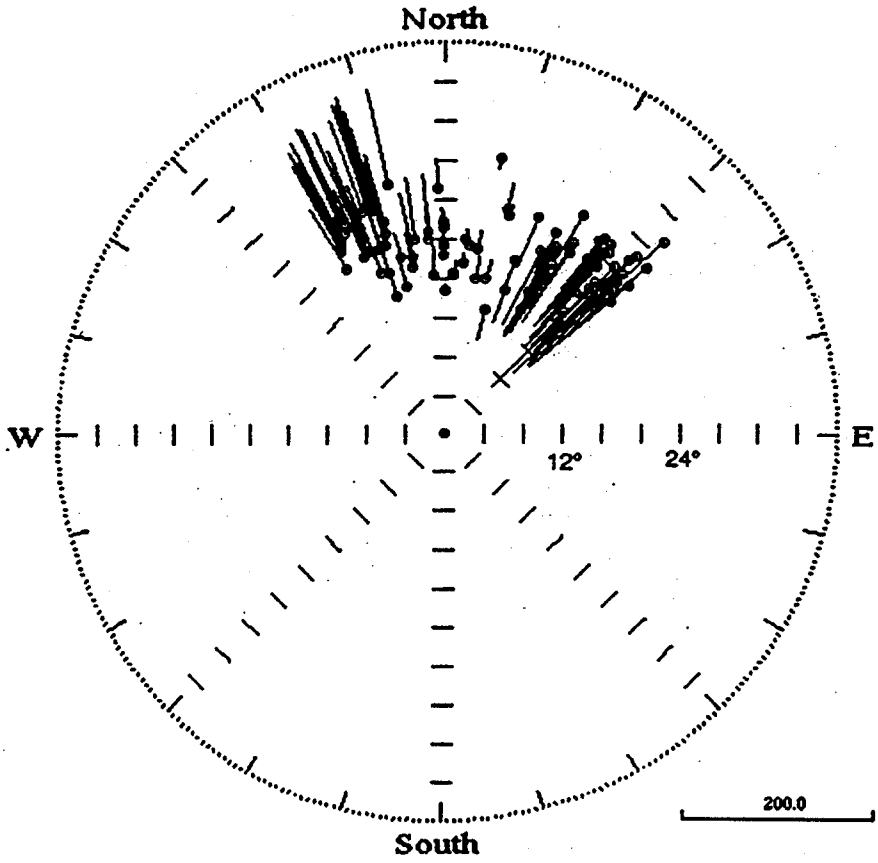

F-region doppler skymap. Millstone Hill, local midnight

Fig. 09c

Sequence of HF Skymaps. Agua Verde 1 Oct. 1994
Sampling Frequency 3.0 MHz

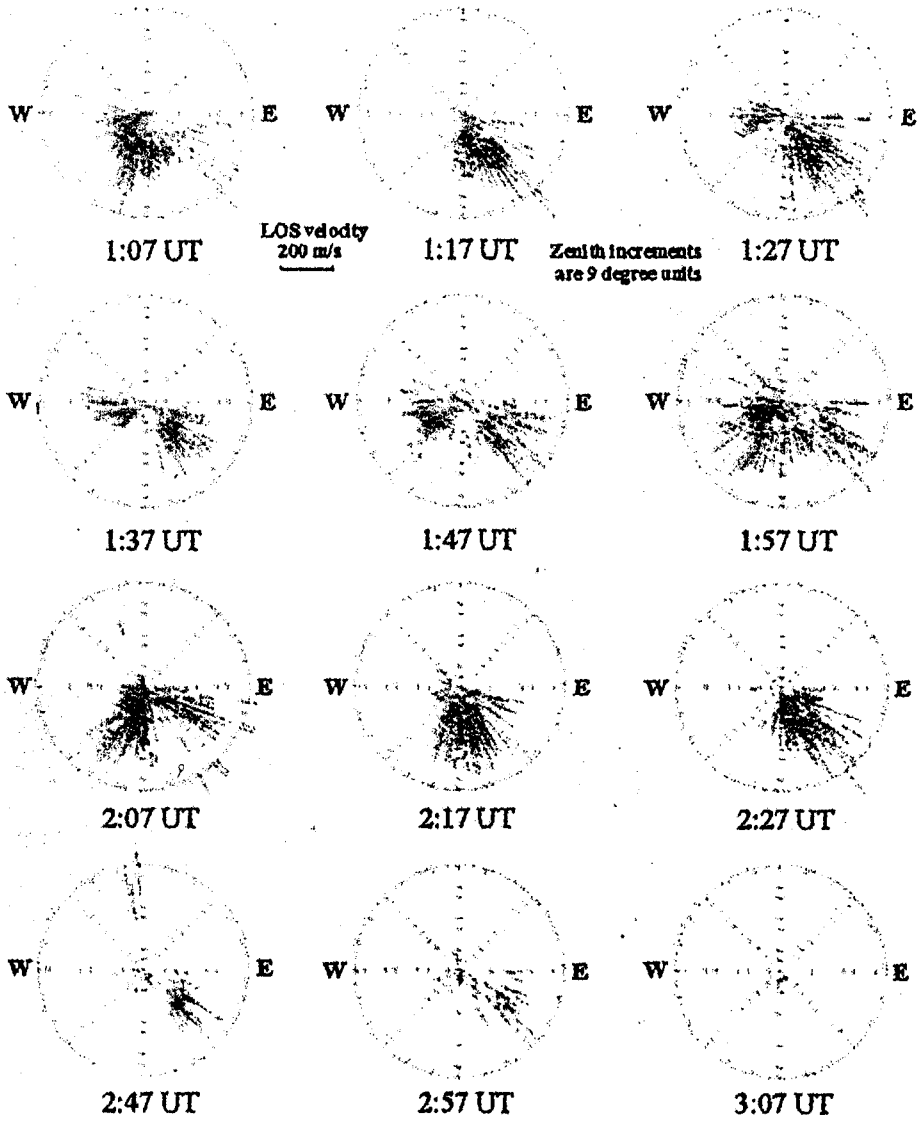

10-min sequence of skymaps at Agua Verde, Chile, on 1 October 1994 starting at 0107 UT. The tick marks on each skymap mark 9° increments in zenith angle. Each skymap represents one 20 s observation. The locations of the individual reflection points are indicated as blue (positive Doppler) and red (negative Doppler) dots, the lengths of the bars are proportional to the line-of-sight velocity.

Fig. 09d

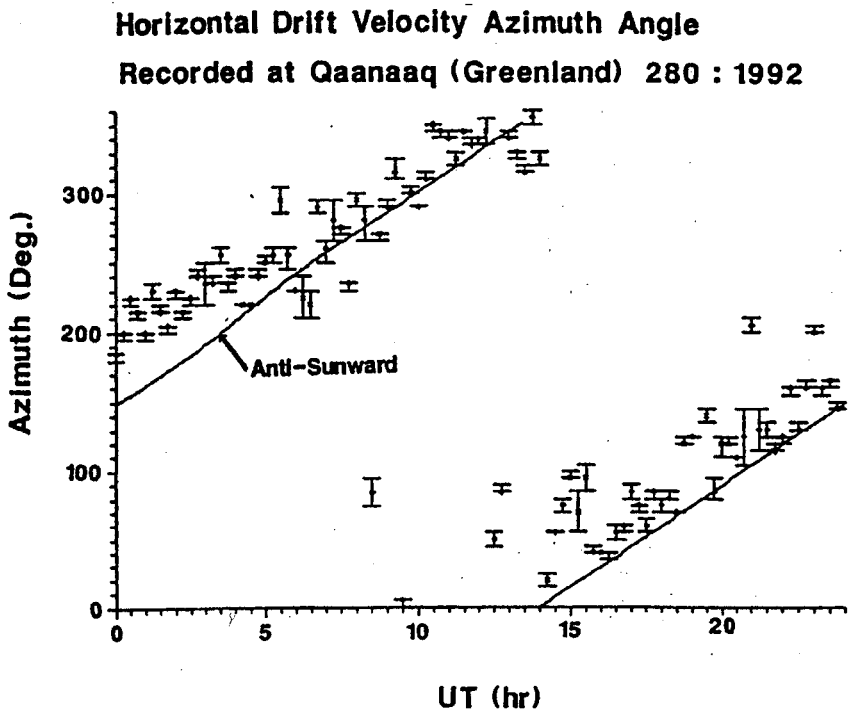

Digisonde measurements of the direction of the *F*-region plasma drift at Qaanaaq, Greenland (87° corrected geomagnetic) for 6th October 1992. The measured azimuth values, shown with their error bars, closely follow the antisunward direction (*solid line*), suggesting a negative *Z*-component of the interplanetary magnetic field (Reinisch et al., 1987)

Fig. 09e

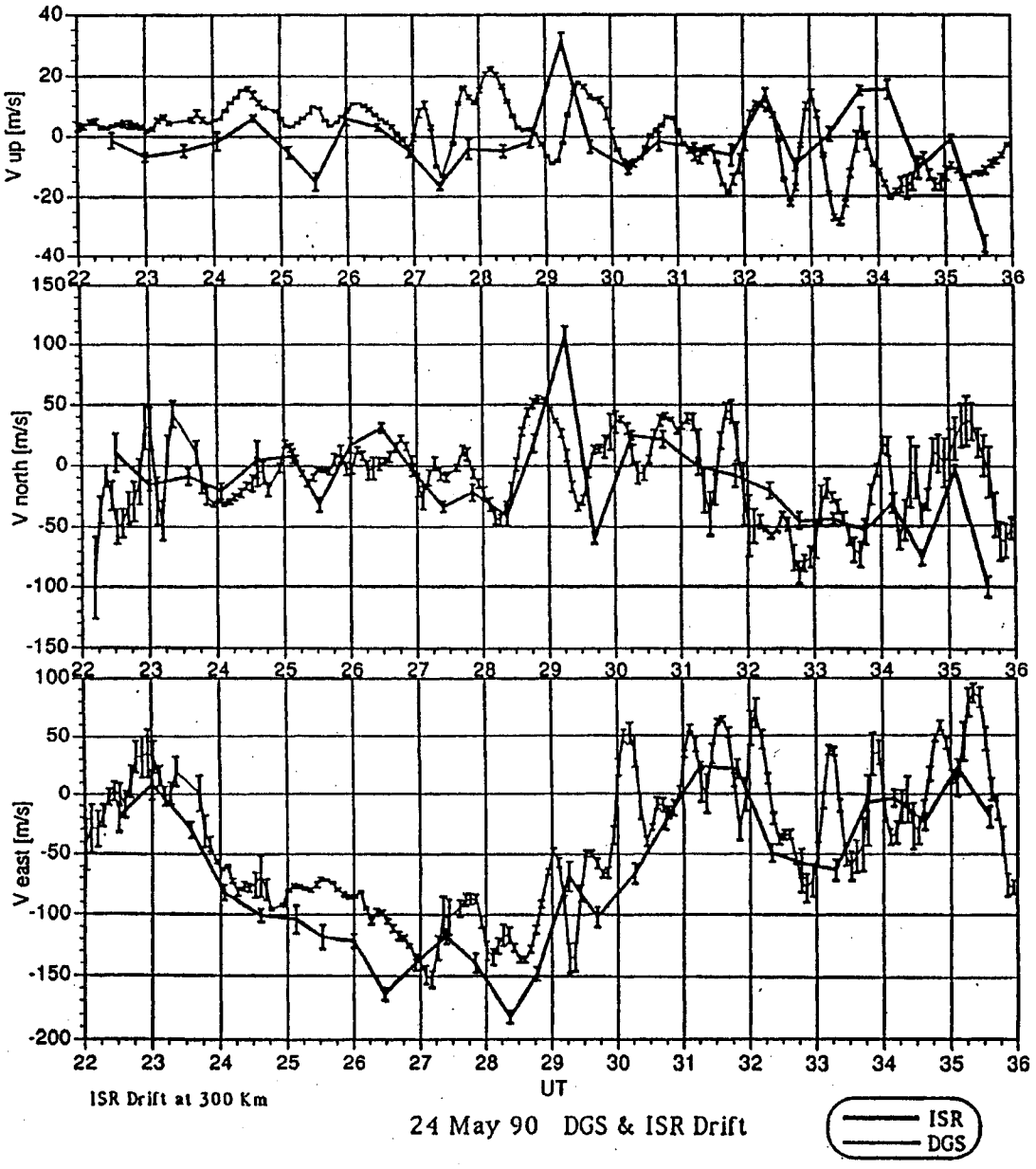

F-region drift velocities at Millstone Hill measured with incoherent scatter radar and ionosonde

Fig. 09f

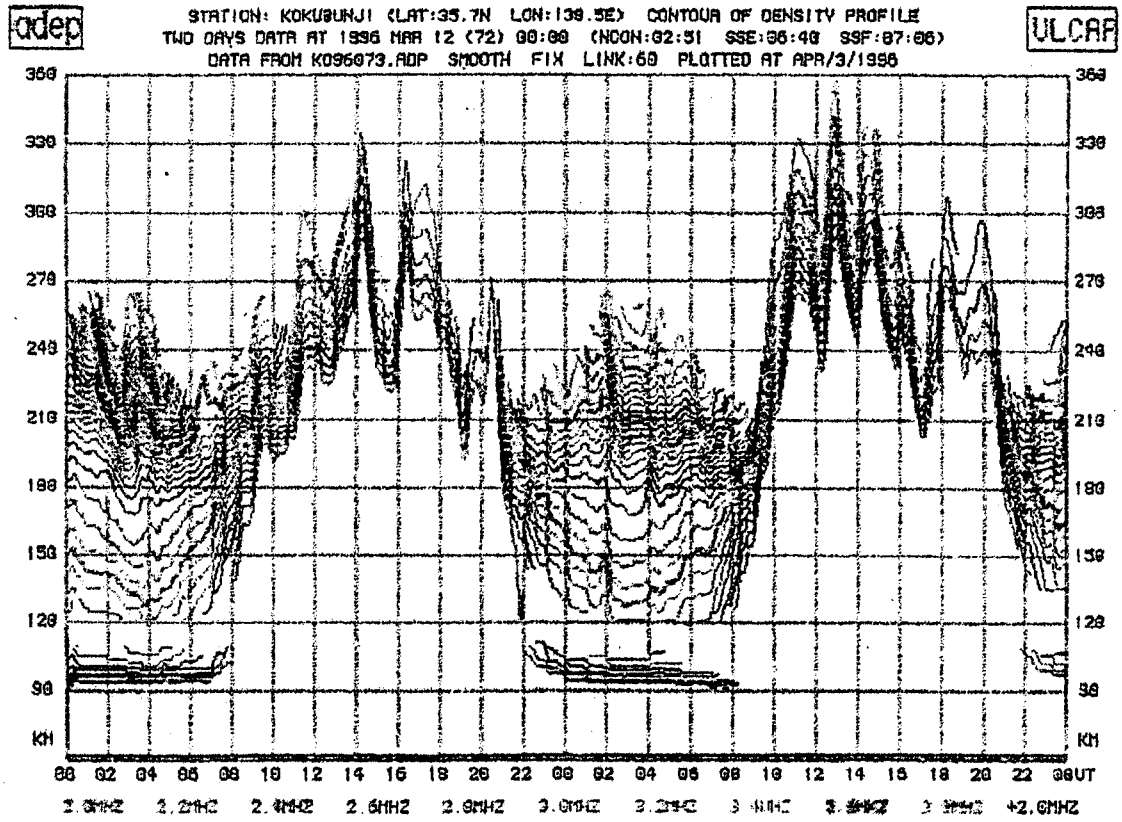

Diurnal variations of electron density contours at Kokubunji, Japan for 12-13 March 1996 (Courtesy, K. Igarashi and J. Scali, PREASA Campaign).

Fig. 09g

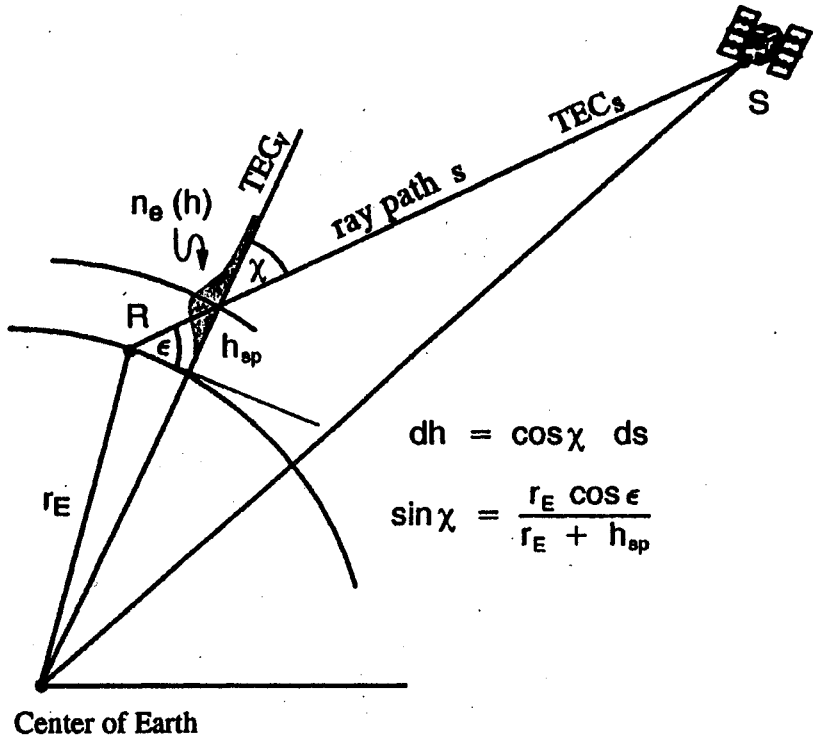

Ray path geometry for trans–ionospheric satellite signals. To derive the mapping function $M(\epsilon)=TEC_s/TEC_v$ a single–layer–approximation for the ionosphere is assumed. The intersection of the ray path with the ionospheric shell at the height h_{sp} defines the location (sub–ionospheric point) of the measurement.

Fig. 10

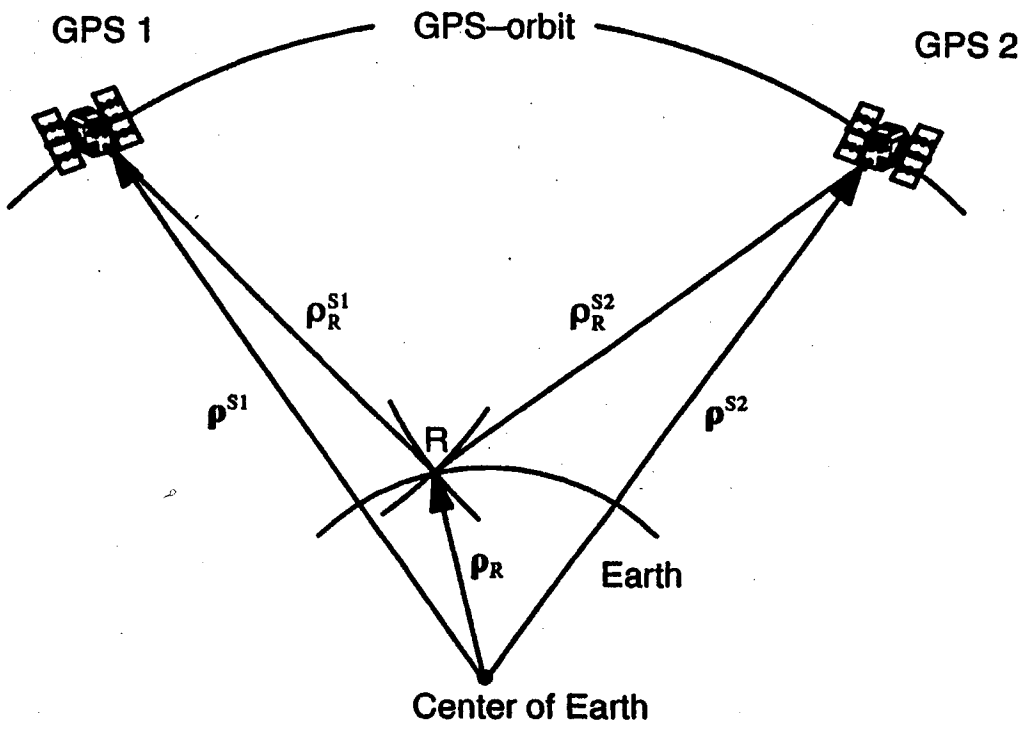

Principle of positioning with GPS.

Fig. 11

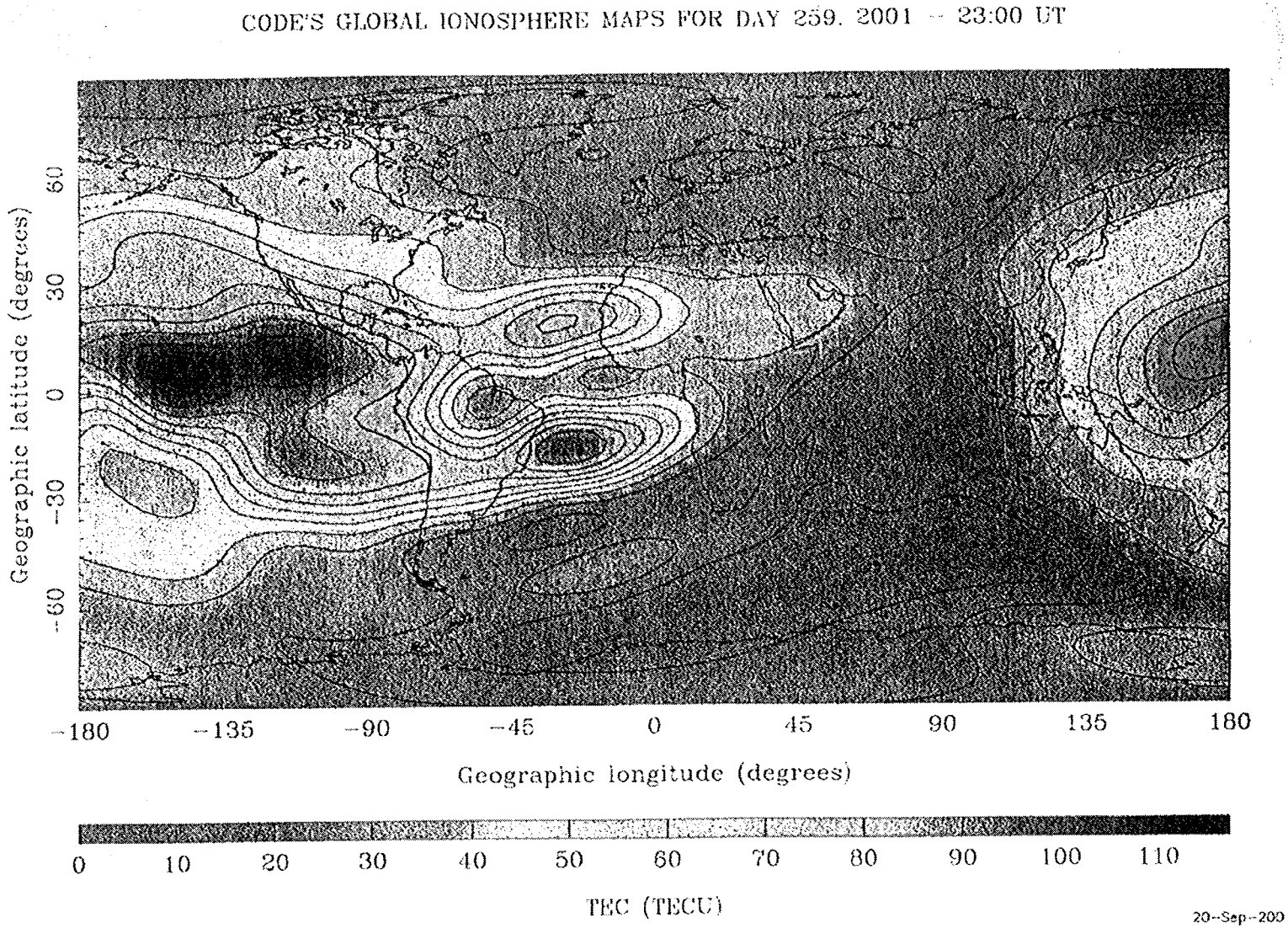
CODE'S GLOBAL IONOSPHERE MAPS FOR DAY 259, 2001 -- 23:00 UT
Geographic latitude (degrees)
60
30
0
-30
-60
-180
-135
-90
-45
0
45
90
135
180
Geographic longitude (degrees)
0
10
20
30
40
50
60
70
80
90
100
110
TEC (TECU)
20-Sep-200

Fig. 12

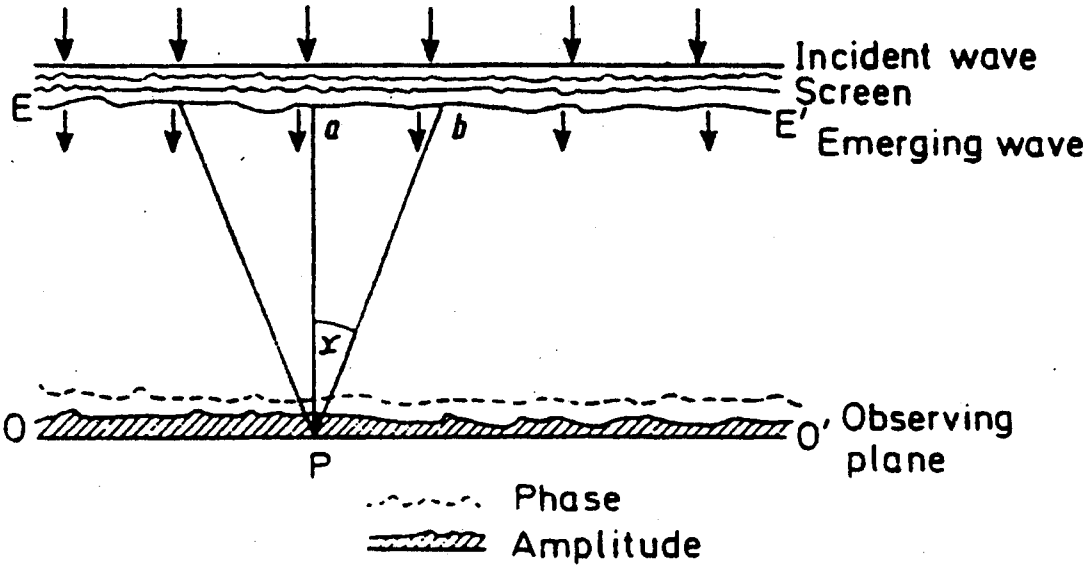

Diffraction of a plane wave incident on a thin phase-changing screen.

Fig. 13

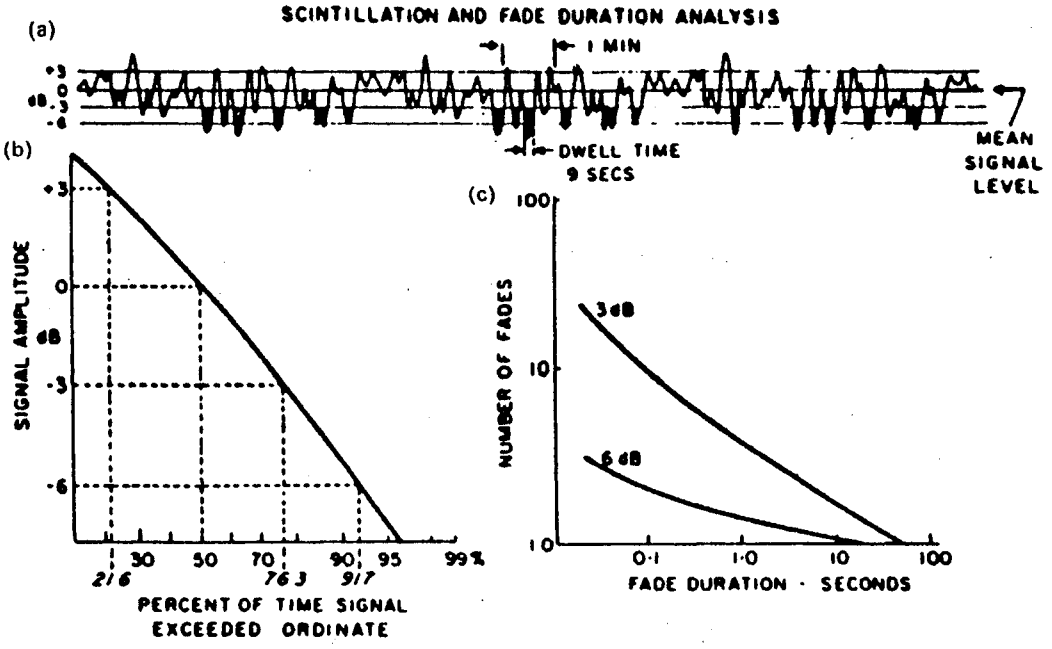

(a) Example of amplitude scintillation, plotted as intensity against time. (b) Cumulative probability distribution. (c) Distribution of fade duration. (After *Handbook of Geophysics and Space Environment* (ed. A. S. Jursa). US Air Force Geophysics Laboratory, 1985)

Fig. 14

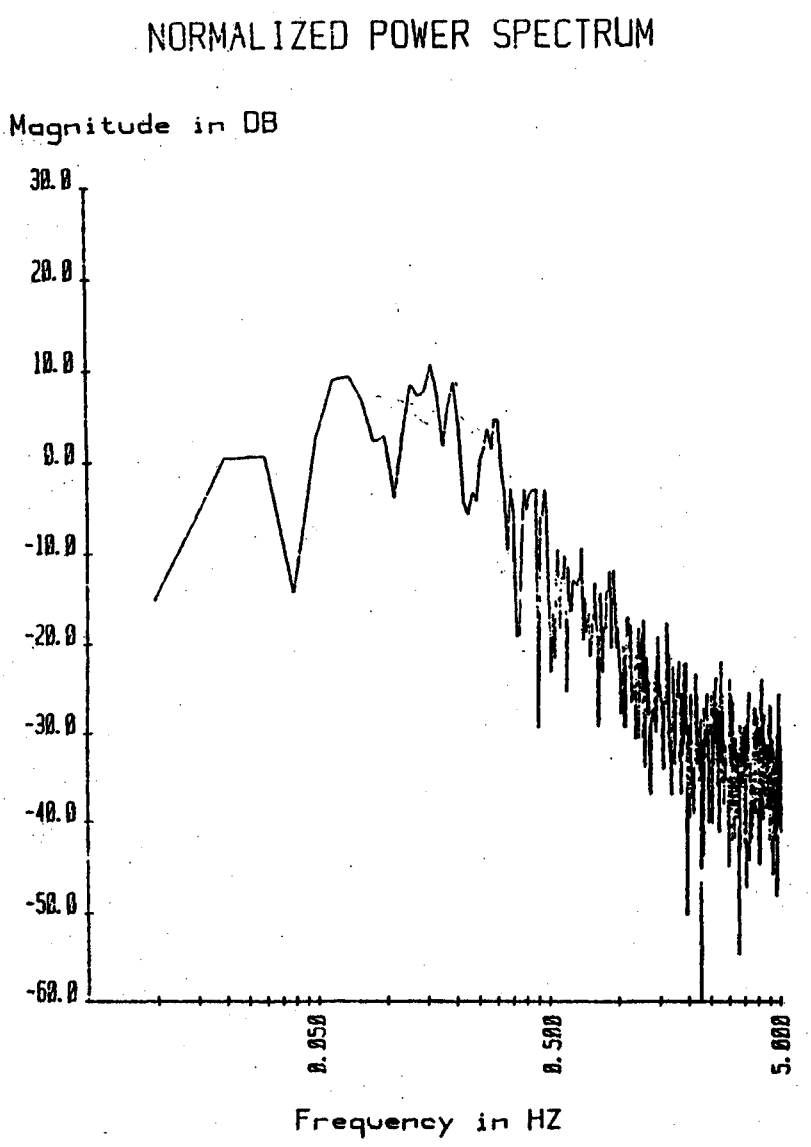

Amplitude power spectrum for the data recorded on September 6, 1977, at one of the stations.

Fig. 15

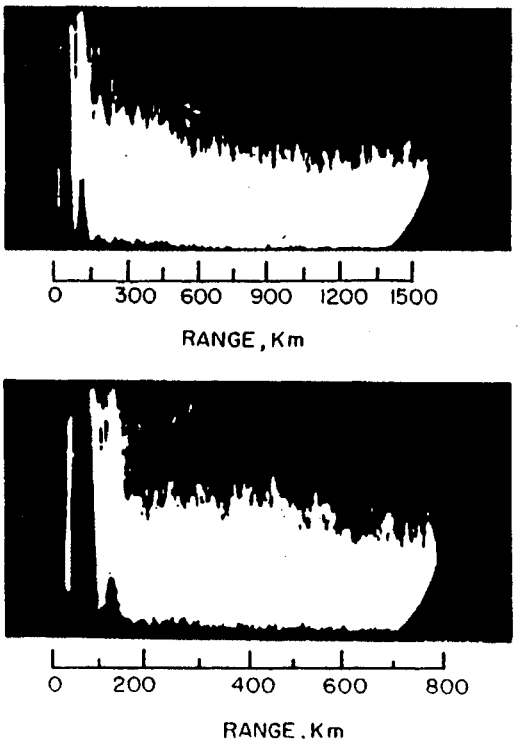

Typical example of data obtained on Bowles' first incoherent scatter radar experiment at Long Branch, Illinois. (Bowles 1958)

Fig. 16a

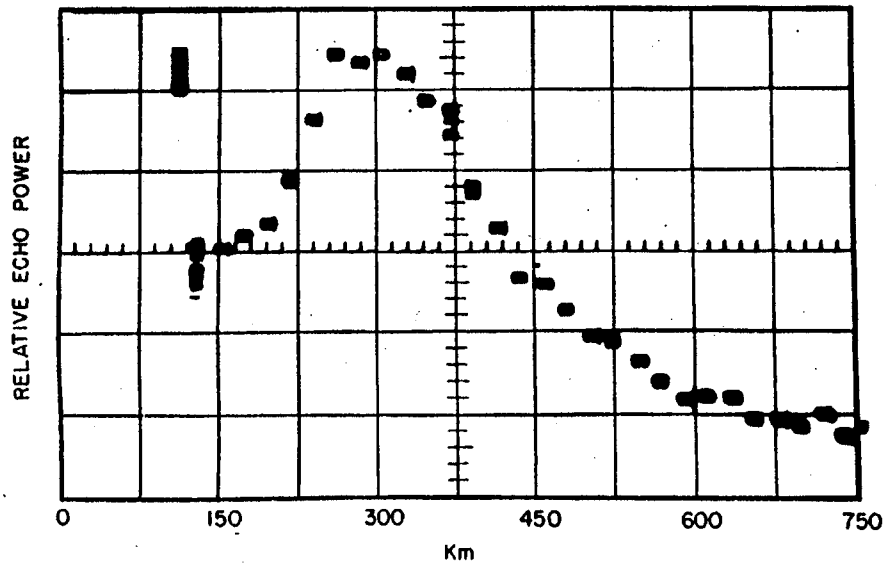

Output of integrator used in Bowles' ISR experiment. (Bowles 1958)

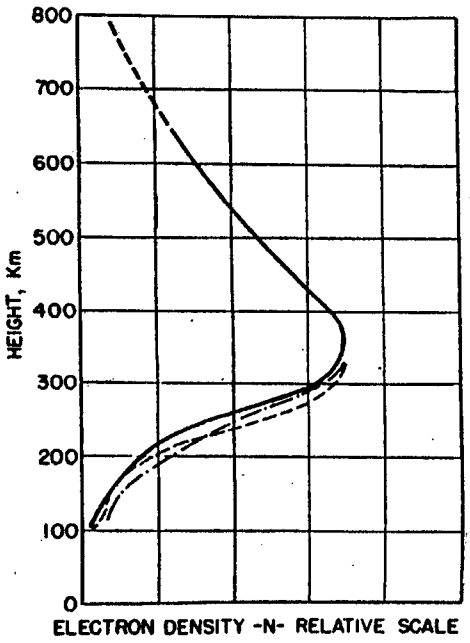

One of the first electron density profiles of the ionosphere obtained using the ISR technique. (Bowles 1958)

Fig. 16b

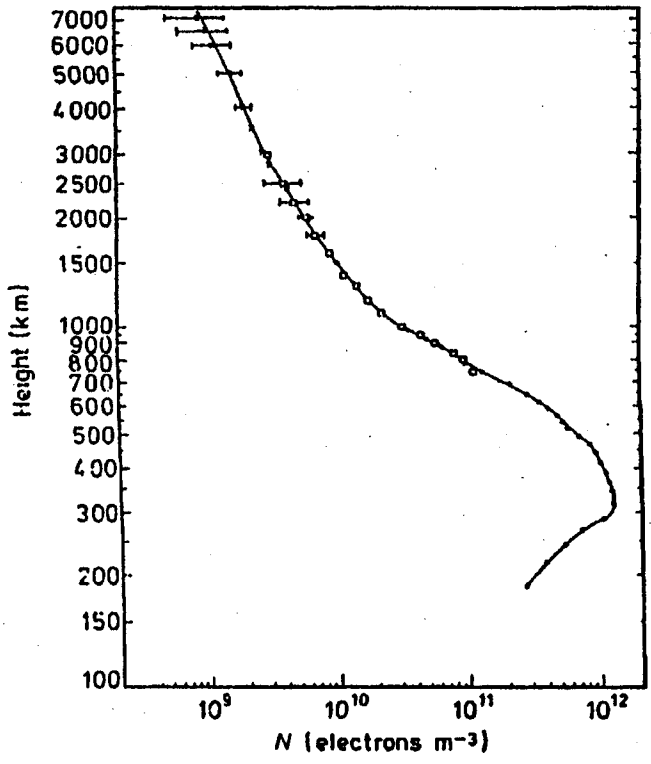

$N(h)$ profiles from 200 to 7000 km at Jicamarca, Peru on 25 April 1962 (after Bowles 1963). ×, 1355 EST; □, 1405 EST; ●, 1415 EST.

Fig. 16c

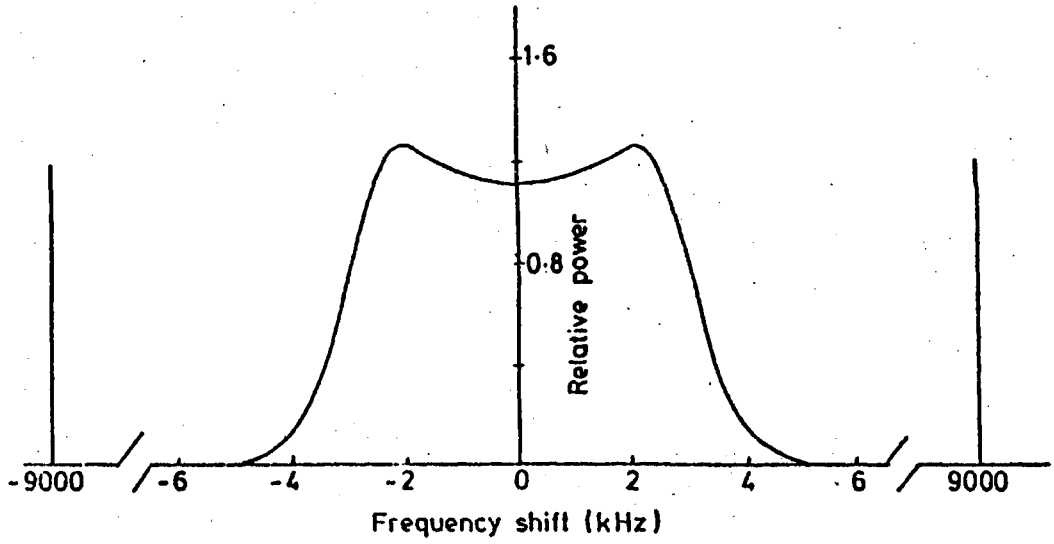

Ion spectrum and plasma (electron) lines for the conditions $N = 10^{12}$ m^{-3}, $T_e = T_i =$ 1000 K, $\lambda = 1$ m, $M_i = 16$. (W. J. G. Beynon and P. J. S. Williams, *Rep. Prog. Phys.* **41**, 909, 1978)

Fig. 17

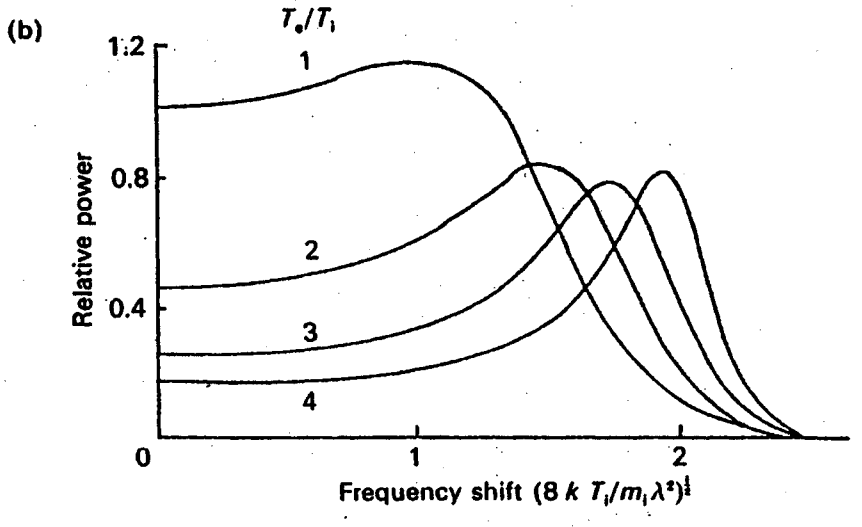

(a) Velocity distribution of thermal electrons $N(v_e)$ and thermal ions $N(v_i)$, and the phase velocity of electron–acoustic (c_e^-) and ion–acoustic (c_e^+) waves. $N(v_e)$ and $N(v_i)$ are normalized so that $N(0) = 1$ in each case. $N = 10^{12}$ m^{-3}, $\lambda = 1$ m, $M_i = 16$, $T_i = 1000$ K, $T_e = 1500$ K (———), $T_e = 2500$ K (·····). (b) Dependence of ion spectrum on T_e/T_i. (After W. J. G. Beynon and P. J. S. Williams, *Rep. Prog. Phys.* **41**, 909, 1978)

Fig. 18

Presently Operational ISR Systems

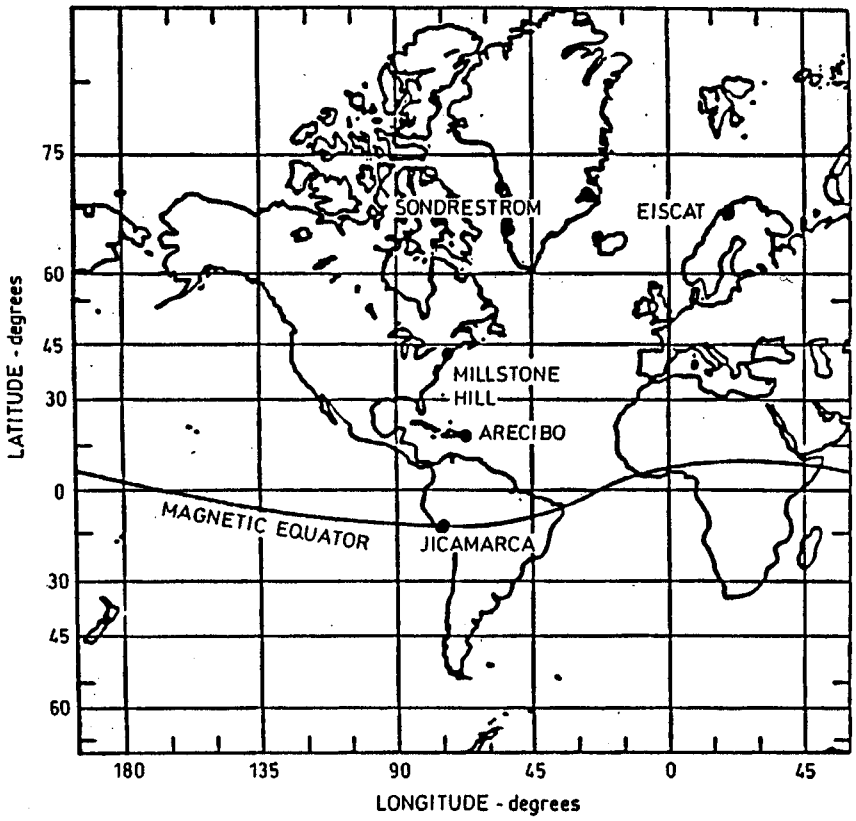

Global distribution of incoherent scatter radar (ISR) systems which are presently operational (1991), excluding the MU Radar in Japan, which is primarily a "middle atmosphere" radar

Fig.19